Confronting Astrophysical Uncertainties in the Direct Detection of Dark Matter

Bradley J. Kavanagh, MSci

Thesis submitted to the University of Nottingham for the degree of Doctor of Philosophy

May 11, 2014

Abstract

Published work

Parts of the work described in this thesis have appeared in the following published works:

1. *Parametrizing the local dark matter speed distribution: a detailed analysis*
   B. J. Kavanagh
   Submitted to Phys. Rev. D, arXiv:1312.1852

2. *WIMP physics with ensembles of direct-detection experiments*
   A. H. G. Peter, V. Gluscevic, A. M. Green, **B. J. Kavanagh**, S. K. Lee
   Submitted to Phys. Dark Universe, arXiv:1310.7039

3. *Model independent determination of the dark matter mass from direct detection*
   B. J. Kavanagh and A. M. Green
   Phys. Rev. Lett. 111, 031302 (2013), arXiv:1303.6868

4. *Improved determination of the WIMP mass from direct detection data*
   B. J. Kavanagh and A. M. Green
   Phys. Rev. D 86, 065027 (2012), arXiv:1207.2039

Acknowledgements

This is dedicated to all of those with big egos
Never fakin', we get the dough and live legal

–Dr. Dre

Contents

List of Figures

List of Tables

Nomenclature

$\sigma_{SI(SD)}$ WIMP nucleon spin-independent (spin-dependent) cross section

m_χ WIMP mass

Chapter 1

Introduction

What and where is dark matter? For a question so central to cosmology and particle physics, the prospects for finding an answer do not at first glance seem promising. As with so many things in physics, we should not by all rights be able to answer the question, nature having hidden itself away in the dark recesses of the universe. But dark matter is all around us and we merely need a window through which to view it. In this work, I will discuss strategies for the direct detection of dark matter: how they offer us a window - however murky - into the dark universe; how they are faced with myriad uncertainties; and how those uncertainties can be overcome to help us to understand more about what dark matter is and how it is distributed in our tiny patch of the universe.

The question '*What is dark matter?*' is perhaps best answered by reviewing the current evidence for its existence. Evidence for dark matter is found on scales from the Milky Way up to the cosmological horizon, with a range of observations which cannot be adequately explained with the observed constituents of the universe. Dark matter is an invisible component introduced to reconcile these observations with the known laws of physics - most importantly, General Relativity. Beyond this general definition, there are a wide range of particle physics candidates which may play the role of dark matter. These typically derive from theories of physics beyond the Standard Model, meaning that the study of the properties of dark matter can shed light on theories of high energy physics. Many of these proposed dark matter candidates have weak but non-zero interactions with particles of the Standard Model, leading to several avenues through which it is hoped the non-gravitational detection of dark matter may soon be achieved.

In this chapter, we summarise the evidence in support of the dark mat-

ter paradigm, including constraints from precision cosmology. We then describe some of the broad classes into which particle dark matter candidates can be categorised, as well as describing a few specific candidates in more detail. Finally, we discuss current progress and constraints from direct and indirect searches for particle dark matter.

1.1 Evidence for dark matter

Dark matter is a key component of the ΛCDM paradigm of modern cosmology. In this framework, the energy density of the universe today is dominated by the constant and uniform contribution of the vacuum, Λ, also referred to as Dark Energy. This contribution exerts a negative pressure and drives the accelerating expansion of the universe which was the subject of the 2011 Nobel Prize in Physics [1, 2]. However, the formation of structure in the early universe is driven by the clustering of an inert, slow moving and as yet undetected matter component [3]: Cold Dark Matter. In ΛCDM cosmology, baryonic matter makes up a much smaller fraction of the energy density of the universe. Cosmological experiments allow us to precisely determine the contributions of these various components (see e. g. WMAP [4], BOOMERanG [5], BOSS [6], BICEP2 [7] and CFHTLenS [8] to name just a few.)

A particularly sensitive probe for determining the dark matter contribution to the energy budget of the universe is the measurement of the temperature anisotropies of Cosmic Microwave Background (CMB) photons. These contain an imprint of the acoustic oscillations of the baryon-photon fluid during the era of recombination. The scale of these oscillations is sensitive to the size of the gravitational potential generated in the early universe by dark matter. **This is shite and needs fixing, am I talking about BAOs or what?** The recent Planck experiment [9] measured the angular power spectrum of these CMB temperature anisotropies. Figure 1.1 shows the results of these measurements, as well as the best fit 6-parameter ΛCDM model. The contribution of the cosmological constant, the total matter component, and the separate baryonic and dark matter components to the total energy density of the universe is shown in Table **??**, constrained with an accuracy of less than 3%. We are lead to the conclusion that ∼84% of the matter content of the universe is in fact dark.

Do more evidence - and less 'problems' - maybe move the

Parameter	68% limits
Ω_Λ	0.686 ± 0.020
$\Omega_m h^2$	0.1423 ± 0.0029
$\Omega_b h^2$	0.02207 ± 0.00033
$\Omega_c h^2$	0.1196 ± 0.0031

Table 1.1: Energy density of the cosmological constant (Λ), total matter (m), and separate baryonic (b) and cold dark matter (c) components in units of the critical density **define...**, as obtained by the Planck Collaboration [10]. The Hubble parameter is defined as $H_0 = 100\ h\,\mathrm{km\ s^{-1}Mpc^{-1}}$.

BBN stuff here? Need to add more CMB and LSS stuff... *Read for details: arXiv:1404.5415*

CFHTLENS: arXiv:1404.5469

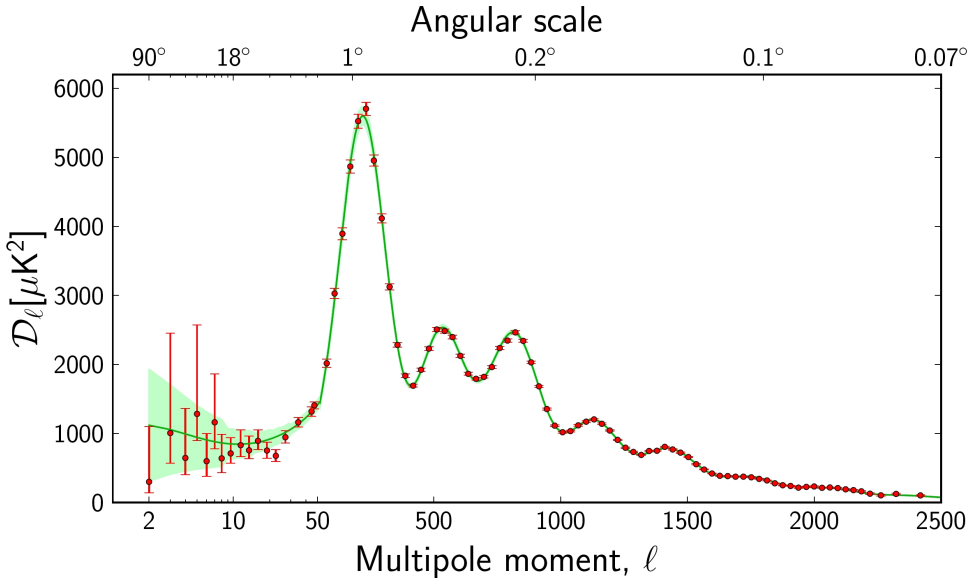

Figure 1.1: CMB anisotropies. **Need actual caption**

However, the evidence for dark matter is not purely cosmological. In 1933, Zwicky measured the velocity dispersion of galaxies in the Coma cluster [11]. An application of the Virial Theorem indicated a gravitational mass in the cluster which was several hundred times bigger than that expected from the luminosity of the member galaxies. It is now known that some of this mass is in the form of hot ($\sim$1 million K), X-ray emitting intracluster gas [12]. Nonetheless, a discrepancy remains; current estimates of the mass-to-light ratio of the Coma cluster give a value of roughly 150 times

that of the Sun [13, 14]. However, the Coma cluster does not appear to be unusual. Measurements of the masses of a large number of galaxy clusters using gravitational lensing [15], X-ray observations [16] and dynamical estimates [17] indicate that a significant fraction of a cluster's mass must be dark.

The validity of the ΛCDM paradigm is also borne out in results from N-body simulations. These simulations track the evolution of structure in the universe by accounting for the dynamics and gravitational interactions **only Newtonian?** of a large number of particles starting from some initial conditions. These may be horizon-scale cosmological simulations, tracing the collapse of the initial density perturbations after decoupling (such as the the Millenium simulation [18]), or galaxy-scale simulations, tracing the formation and growth of a small number of galaxies starting from initial conditions at intermediate redshift (such as the Via Lactea [19] and Aquarius [20] simulations).

Maybe swap this paragraph with the next one - it makes more sense? A variety of sophisticated computational techniques (such as smoothed particle hydrodynamics [21], adaptive mesh refinement [22] and moving mesh cosmology [23]) have been employed and refined to make such simulations computationally feasible and to allow higher and higher resolutions to be reached. In spite of this, computational limitations mean that the highest resolution simulations still use 'particle' masses of the order of $10^5 M_\odot$ [24], many orders of magnitude more massive than the O(GeV-TeV) particles expected to make up the universe's dark matter. **say more...**

Many N-body simulations are DM-only, simulating only the gravitational dynamics of collisionless particles. However, an increasing number are incorporating baryonic physics such as gas dynamics, as well as stellar evolution, chemical enrichment and a variety of feedback processes **Need some citations...**. Appropriately accounting for these factors is extremely complex and in some cases the strength of these processes is unknown and must be tuned in the simulations to match observations (see for example Ref. [25]). **Mention some other problems - shock resolution etc.** Due in part to these difficulties, the impact of baryonic physics on the formation of galaxies and the properties of DM haloes is still uncertain (see for example Refs. [24, 26]). I will revisit this topic - and its consequences for the direct detection of dark matter - in Chapter **??**.

In spite of these limitations, a consistent picture has emerged from a vast array of N-body simulations. The size distribution of gravitational structures found in the universe is well matched over a range of distance scales with that obtained from N-body simulations **CITATION!**. In particular, the fact that DM is non-interacting means that it begins to collapse gravitationally earlier in cosmic time than baryonic matter. After decoupling, baryons then fall into the gravitational wells produced by the infalling DM structures. Without DM, the baryonic matter in the universe could not have had enough time to collapse to form the array of gravitationally bound structures we see today [3]. **Coldness...**

N-body simulations also suggest that galaxies such as the Milky Way should be embedded in a large, approximately spherical dark matter halo. This is corroborated by observations of the rotation curves of spiral **just spirals?** galaxies. In particular, the circular velocity of stars in these galaxies is observed to be approximately constant out to large galactocentric distances [27, 28]. This is shown schematically in Fig. 1.2. **Say something about gas, and 21cm emission (so that you can check the rotation beyond the luminous matter). [Optical edge]** The majority of the mass of the luminous disc is concentrated at small radii, suggesting that there should be a Keplerian decay of the circular velocity at large radii: $v \sim r^{-1/2}$. However, the inclusion of a non-luminous dark matter halo can reconcile this expectation with the observed flat rotation curves. The density profiles $\rho(r)$ required to provide a good fit to rotation curve data are consistent with those obtained from N-body simulations, such as the Navarro-Frenk-White profile **Is this really true? Cusp/Core problem?**

$$\rho(r) = \frac{\rho_0}{r/R_s(1 + r/R_s)^2}\,, \tag{1.1}$$

which is described by the central density ρ_0 and a scale radius R_s. This provides a good cross-check between the results of N-body simulations, which span scales up to the cosmological, and galactic-scale observations of the local universe. The rotation curve of the Milky Way itself has also been studied **[cite Mattia and others self-consistent distribution guys]**, as well as the ultralocal distribution of dark matter near the Sun's position. An understanding of this distribution has significant implications for the study of dark matter detection and we defer a detailed discussion

to Chapter ??.

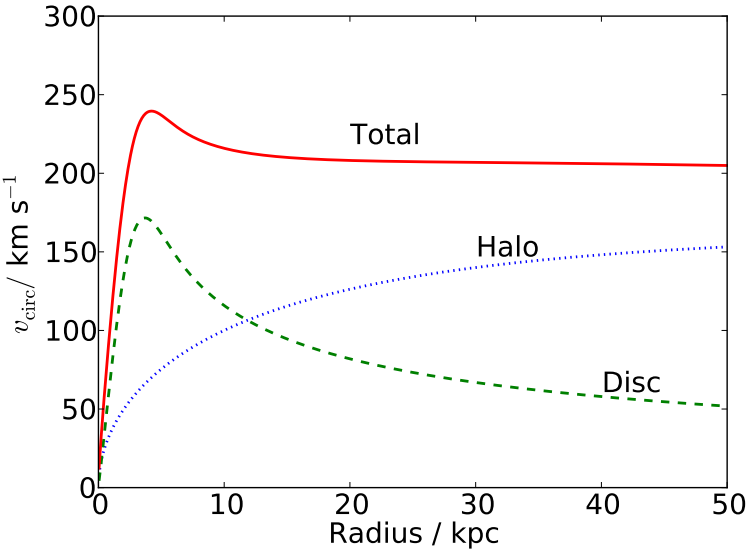

Figure 1.2: Schematic illustration of galaxy rotation curves (circular velocity as a function of galactocentric distance). The contribution to the circular velocity from the luminous disc (green dashed line) and dark matter halo (red dotted line) are shown, as well as the total circular velocity (solid blue line).

We see that evidence for dark matter appears over a wide range of distance scales, from the cosmological horizon down to our own Milky Way. Dark matter is required to explain the formation and growth of large scale structure, the dynamics of both galaxies and galaxy clusters and the anisotropic temperature distribution of the CMB among others. In spite of this, there remain several problems and unanswered questions with the dark matter paradigm.

Cite Lyndzo! Lensing Tully-Fisher Bullet cluster

1.1.1 Problems with dark matter

There have emerged several issues with the dark matter dominated model of structure formation as studied with N-body simulations. For example, DM-only simulations predict the existence of a large number of massive subhalos around Milky Way-size galaxies [20]. Using semi-analytical models of galaxy formation Kauffmann et al. [29] predicted that a Milky Way-size halo should host over 100 subhalos massive enough to support observable satellite galaxies. However, the known population of dwarf

spheroidal (dSph) satellite galaxies for the Milky Way is on the order of 20 [30], although more ultra-faint satellites are still being discovered (e.g. see Ref. [31]). This discrepancy between the predicted and observed amount of substructure in CDM structure formation is often referred to as the 'missing satellite problem' [32].

A related issue is the so-called 'too big to fail' problem, which concerns the density of dark matter subhalos. In particular, it is found that the most massive DM subhalos found in N-body simulations are too massive to host the brightest of the Milky Way's dSph satellites [33]. If the observed dSph galaxies are hosted instead by less massive subhalos, this leaves a large number of more massive DM halos which have not yet been accounted for [34]. **NB: there are 11 well-known/bright/classical dSph satellites...**

Finally, there is also a discrepancy between the observed and simulated density profiles: the 'Core-Cusp' problem (for a review, see Ref. [35]). Cosmological simulations indicate that the DM density should be sharply peaked near the centre of low surface brightness and dSph galaxies [36, 37]. In contrast, observations of the rotation curves of a large number of galaxies suggests the presence of a core - a flat dark matter density profile near the centre [38, 39]. While these results are still under contention (for example, Ref. [40] find rotation curves consistent with *cuspy* density profiles), they may indicate a significant difference between the process of structure formation in the universe and that extracted from ΛCDM simulations.

A number of possible solutions to these issues have been suggested. Baryonic effects such as dynamical friction and stellar and supernova feedback (see for example Refs. [41–43]) can lead to the expulsion of DM from the centres of subhalos, reducing the total halo mass and leading to a flatter central density profile. **This bit could be better.** Others have suggested that a *warm* dark matter model may be a better fit to the data [44–46], reducing the amount of structure on small scales, as described in Sec. 1.2. **What about solutions about increasing the resolution of N-body simulations?** Whatever the ultimate resolution of these problems, it is clear that dark matter dominated structures such as dSph galaxies are testing ground for an even more precise understanding of structure formation in the DM paradigm.

There remains one problem which is of a much more theoretical nature.

Dark matter is invoked to account for missing mass in a wide range of scenarios. However, this missing mass has not yet been observed indicating that it must interact only very weakly with photons and other particles of the standard model. In fact, as we shall see in Sec. 1.2, there is strong evidence that particles making up the universe's dark matter cannot be baryonic and must originate from beyond the Standard Model of particle physics. In the next section, we investigate what more can be inferred about the nature of particle dark matter and explore some well-motivated candidates.

MACHOs? MOND?

1.2 Properties of dark matter

Beyond its gravitational contribution to the universe, we appear to know little about the nature of particle dark matter. However, the success of modern cosmology and the lack of a confirmed detection so far means that we do have a grasp on some of the properties of any potential candidate. Taoso et al. [47] present a '10-point test' which must be passed by any particle before it can be considered as a viable dark matter candidate. Here, I will briefly discuss four of these points, namely, that the DM candidate must be cold, neutral, produced with the appropriate relic density and compatible with primordial nucleosynthesis. **What about stability? THIS IS IMPORTANT FOR CANDIDATES - mention...**

1.2.1 Coldness

Results from N-body simulations indicate that dark matter should be *cold*. That is, DM should be travelling non-relativistically when it decouples from the thermal bath in the early universe. **Not quite true - could be warm...** In practise, this typically means that it cannot be have a mass greater than around 1 keV [48]. **Watch out - this is actually the limit of WDM...** The typical speed of DM particles in the early universe defines the so-called *free-streaming length*. Below this length-scale, density perturbations are suppressed due to Landau damping [49]. For non-relativistic species, this free-streaming length scales as $m_\chi^{-1/2}$ for thermal relics of mass m_χ [50] **Why even say this...?**. For particle candidates which are too light - and which therefore travel too quickly after decoupling

- small scale structures cannot form and cannot match the distribution of structures we see today. **Distinguish between warm and cold - what is the length scale?** *Warm* dark matter candidates with keV-scale masses have been suggested to explain the subhalo structures at the scale of dSph galaxies (as has already been discussed) However, *hot* dark matter, which decouples at relativistic speeds, is strongly-constrained and cannot make up more than around 1% of the total dark matter component [51, 52].

1.2.2 Neutrality

The possibility that charged massive particles (CHAMPs) may account for dark matter was proposed by De Rujula et al. [53]. Such particles be free and stable or may instead bind with electrons or positrons to form heavy neutral hydrogen-like objects. However, null searches for anomalous hydrogen in sea water [54] and anomalous heavy elements [55], as well as searches for CHAMPs in cosmic ray experiments [56] indicate that CHAMPs must be present in negligible densities in the Milky Way for masses in the range $10 - 10^8$ GeV. **What about current constraints on 'dark atoms'?** Millichared DM is also strongly constrained. Searches for neutrino magnetic moments in reactor experiments exclude DM with charge greater than $10^{-5}e$ for keV-scale masses and below [57]. Searches for distortions in the CMB caused by the interactions of millicharged particles limit the DM charge to be less than $10^{-7}e$ for masses of 1 eV and below [58].

Could DM particles carry a colour charge? In this case, DM particles would interact strongly with particles of the SM. Such strong interactions may disrupt galaxy formation [59], distort the CMB due to scattering off baryons [60] and have been strongly constrained by experimental searches with the X-ray Quantum Calorimeter [61] and direct detection experiments [62]. **What about weak hypercharge?**

We are left with the conclusion that (without a mechanism for evading the above constraints [**?**]) DM particles must carry no (or almost no) conventional electromagnetic, weak or strong charge. This rules out all SM particles **(does it...?)** as accounting for DM hinting strongly that these particles must derive from theories of physics beyond the Standard Model.

1.2.3 Relic density

In order to account for the dark matter in the universe, a good candidate must be produced in the early universe with sufficient abundance to match the currently observed value $\Omega_c h^2 0.1196 \pm 0.0031$ (see Table 1.1). If produced with a smaller abundance, the candidate cannot account for the entirety of the universe's dark matter (though it could still contribute, along with other candidates, as in Ref. [63]). If on the other hand, it is produced with too great an abundance, it could threaten to exceed the DM density constraint set by Planck and overclose the universe.

Depends on coldness

The standard scenario for the production of dark matter is referred to as thermal freeze-out [3]. In this scenario, DM particles remain in kinetic and chemical equilibrium with SM particles in the very early universe by scattering and annihilation processes. Their abundance follows a Maxwell-Boltzmann distribution $n \sim (m/T)^{3/2} \exp(-m/T)$ for a mass m and temperature T. As the universe expands, however, the particles become diluted, reducing the interaction rate **actually, the annihilation rate?** until eventually the DM particles become decoupled from the SM particles and are 'frozen-out.' They are then left with the abundance they had when they decoupled, which is further diluted by the expansion of the universe to become the abundance we see today. The exact relic abundance depends on $\langle \sigma_{\text{ann}} v \rangle$, the average annihilation cross section of the DM particles (weighted by the DM speed). If this is small, DM will decouple early when the temperature of the universe is still high, leading to a large relic abundance. If the annihilation cross section is large, DM will remain in equilibrium for longer, even as the particles become more and more diluted. The DM then freezes out later, with a lower temperature and lower relic abundance. This process is illustrated schematically in Fig. **??**. *Make a simple figure for this.* The resulting relic abundance for GeV-scale DM is given approximately by:

$$\Omega_c h^2 \approx \frac{3 \times 10^{-27} \text{ cm}^3 \text{ s}^{-1}}{\langle \sigma_{\text{ann}} v \rangle}, \tag{1.2}$$

leading to a canonical value of around $\langle \sigma_{\text{ann}} v \rangle \approx 3 \times 10^{-26}$ cm^3 s^{-1} for the annihilation cross section. This coincides well with the value expected for particles with weak-scale interactions (so-called weakly interacting massive particles, or WIMPs), leading some to refer to this argument as the WIMP

miracle. **(Add in refs from page 121 of PDM.)** In reality, the full differential equations describing the DM number density must be solved [64], accounting for co-annihilations [65], which may boost the total cross section. However, the simplicity of this scenario make cold thermal relics an attractive candidate for DM.

Dark matter may also achieve the correct relic abundance through a variety of other mechanisms. 'Freeze-*in*' [66] involves particles which interact so weakly (termed feebly interacting massive particles, FIMPs) that they never reach equilibrium. Instead, a relic population is built up gradually through the production of FIMPs by annihilation of SM particles. In contrast to the freeze-out scenario, the relic abundance of FIMPs increases with increasing annihilation cross section. Dark matter may also be produced gravitationally from vaccuum fluctuations during and after inflation [67, 68] or from the decays of heavier meta-stable particles (e.g. Refs [69**?**]). These possibilities open up the range of candidates which may be considered to include much lighter or much heavier particles than the freeze-out scenario alone might allow.

1.2.4 Primordial nucleosynthesis

Need more refs here...

Primordial nucleosynthesis (or Big Bang Nucleosynthesis, BBN) describes the production of light nuclei in the first few minutes after the big bang. By solving a set of coupled Boltzmann equations describing the nuclear reactions of protons, neutrons and light nuclei, we can obtain the primordial abundances of these light nuclei and compare with the inferred values. **Citation** Significantly, these abundances depend strongly on the baryon-photon ratio η and therefore the total baryon density. Fits to data lead to the result $\Omega_b h^2 = 0.017 - 0.024$ [70], independent of the value obtained from CMB measurements (Table 1.1). Thus, the dark matter of the universe cannot be baryonic. **Combine this with the 'neutrality' constraint and we see that there are no SM particles (or their spartners?) with the correct quantum numbers.** We are led to conclude that particle dark matter must consist of some as-yet undiscovered particle. **Link this to the next section...**

The results of BBN are also very sensitive to light new species, which can alter the number of relativistic degrees of freedom in the early universe

and therefore affect the expansion rate. These include, for example, gravitinos [71], right-handed neutrinos [72] and millicharged particles []. BBN therefore provides strong constraints on the parameters of such models. **What about stating some of the constraints on Nv?** In addition, the decay of dark matter particles into electromagnetic or hadronic showers during nucleosynthesis can drastically change the primordial abundances of the light elements. BBN can therefore be used to constrain models in which dark matter undergoes early decays (or in which dark matter is produced by the decays of heavier particles) [73].

1.3 Particle dark matter candidates

Make an explicit distinction between WIMPs and non-WIMPs?

While *valid* DM candidates need only satisfy the conditions and constraints which have already been discussed, *well-motivated* candidates should derive sensibly from some as-yet undiscovered theory of physics. In fact, dark matter candidates can be found in a wide range of models of particle physics beyond the standard model. As has already been discussed, massive particles with GeV-scale masses and weak-scale interactions are attractive for obtaining the correct DM relic density. Such a WIMP candidate may be provided by the lightest supersymmetric particle (LSP) in supersymmetric theories [74]. In supersymmetry, each of the known SM particles has a supersymmetric partner (or 'spartner'), with bosons having fermionic partners and vice versa - this additional symmetry is often invoked to help alleviate the hierarchy problem [75]. In models which possess R-parity **[say more?]**, particles carry R-parity 1 while supersymmetric particles ('sparticles') carry R-parity -1. This means that the lightest sparticle cannot decay into SM particles and is therefore stable, making it a promising DM candidate.

Does this hold JUST for the MSSM?

Depending on the parameters of the supersymmetric theory, there are many possibilities for which sparticle will be the LSP. One popular and well-studied possibility is the neutralino χ [76**?**], which is a linear combination of the neutral supersymmetric partners of the W, B and Higgs bosons **[These are the CP-even higgsinos of the MSSM]**. The properties of the neutralino can vary dramatically depending on the mixing between these different components and the underlying supersymmetric parameters

[77] **[This is a bad citation...]**. *Neutralino pros and cons...* In different scenarios **which are...?**, the LSP may be sneutrino [78], a partner of the standard model neutrino. *Say more about sneutrinos...are they excluded already by direct searches?* Another alternative is the gravitino, in which case it may be produced gravitationally in the early universe with a mass greater than 10^{12} GeV, leading to the title 'WIMPzilla' [79].

WIMPs also arise in theories of universal extra dimensions, in which the additional dimensions are compactified, leading to a tower of excited states of the standard model particles [80]. These 'Kaluza-Klein' (KK) particles also possess a KK-parity, which means that the lightest KK particle (LKP) is stabilised [81]. One possibility for the LKP is the first excitation of the B weak hypercharge boson, $B^{(1)}$. In this case, the WIMP would be a spin-1 particle with a mass of around 1 TeV (in order to be produced thermally with the correct relic abundance) [82]. However, it has also been shown that the first KK excitations of the photon and neutrino are viable DM candidates if they also have masses at the TeV scale [83]. In contrast to the LSP, the LKP is described by a relatively small parameter space and may be more easily constrained by upcoming experiments [84].

In light of the problems with models of dark matter structure formation on small scales, there are several candidates which may be attractive for constituting warm dark matter. While standard neutrinos (with masses of a few eV [85]) cannot account for a large fraction of the dark matter **[see earlier]**, keV-scale sterile neutrinos may be viable [86]. Sterile neutrinos interact with ordinary matter via neutrino mixing rather than via electroweak interactions. **[Constraints in Ref.59 of http://arxiv.org/pdf/0903.4849v4.pdf]** While attractive for providing warm dark matter, non-thermal production [87] or multiple sterile neutrinos species [88] may be required to avoid many of these constraints.

Another non-WIMP candidate is the axion. The axion was originally introduced by Peccei and Quinn [89] to solve the strong CP problem. It was observed that this spin-zero particle should be produced in abundance in the early universe via the 'misalignment mechanism' and, for masses in the range $10^{-5} - 10^{-3}$ eV, can account for the cosmological dark matter [90]. It was recently noted that axion dark matter would thermalise and form a Bose-Einstein condensate, acting as cold dark matter at late times [91], as well as explaining anomalies in the alignment of CMB multipoles [92]. Also of interest are a axion-like particles (ALPs), which emerge naturally in

string theory and are expected to span many orders of magnitude in mass and coupling strength [93]. **[Be more explicit about mass ranges.]**

As is clear from this discussion, there are a wide range of well-motivated candidates for the dark matter in the universe. Some further examples include **[list some...] WIMPless dark matter, mirror dark matter,...**, as well as minimal approaches to DM [94]**and others...**. In this work, we focus on the WIMP, not only because of its popularity and generic nature, but because of the large number of experimental searches which provide sensitivity to WIMP dark matter.

[Some overlap here in text...] The final condition appearing in the '10-point test' of Taoso et al. asks the question 'Can it be probed experimentally?' While there are viable DM candidates which interact only gravitationally (such as **WHAT?**), a wide variety of proposed candidates can interact (however weakly) with the particles of the standard model. While the experimental accessibility of a given DM candidate is not a strict necessity, it allows models to be tested (and either falsified or confirmed) beyond the hypothesis stage. In the next section, we explore the different avenues by which models of particle dark matter may be probed.

1.4 Detection of dark matter

Many of the candidates which have been discussed are expected to interact weakly with the particles of the Standard Model. Dark matter particles which are produced by thermal freeze-out in the early universe must have interactions with SM **[Define SM somewhere]** particles in order to maintain thermal and kinetic equilibrium. These interactions are mediated by Feynman diagrams which can be represented (schematically) as in Fig. 1.3. The existence of production, annihilation and scattering processes between DM and SM particles provides a window into the possible detection of particle DM. Each of these processes leads to a distinct detection strategy, often referred to as collider, indirect and direction detection.

1.4.1 Collider production

Elaborate and actually explain more of this section. Add more from the PDM... What about actual current limits, nothing seen yet? What about kinematic endpoints...?

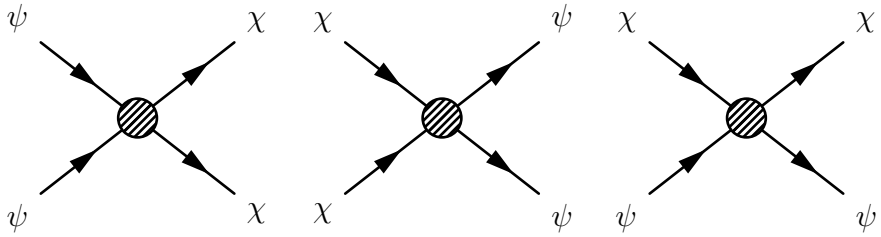

(a) Production (b) Annihilation (c) Scattering

Figure 1.3: Schematic interactions between dark matter particles χ and standard model particles ψ.

Searches for dark matter at the LHC **[What about LEP/Tevatron?]** rely on processes such as Fig. 1.3(a), in which SM particles annihilate to produce dark matter particles. However, the weak interactions of the DM means that once produced, it will escape the detectors of ATLAS and CMS. Thus, collider searches for dark matter must look for other signatures.

One approach is to look for signatures which are characteristic of a particular theory. For example, looking for evidence of KK states which are expected in theories of universal extra dimensions [95, 96], or searching for particle signatures from decay chains which are expected from supersymmetry [97, 98]. While this allows for tight constraints to be placed on specific models, the range of models may be large, making this approach unfeasible. **This is a bit harsh...**

An alternative approach is to look for deviations from the SM expectation and use this to place limits on the operators of an effective field theory [**?**]. One possible signature is to look for the pair production of DM states, with initial state radiation of a SM particle. Combining the possibilities for what is in this initial state radiation (quarks, gluons, photons, Zs, etc.), we can perform a so-called **mono-everything** search [99]. **Mention actual results and mention effective operators...** It is also possible to look for more general missing energy signatures [100], in which energy is carried away by the dark matter particle produced. **So far nothing has been observed.**

One advantage of the effective operator approach is that these bounds can be translated into limits on signals at direct and indirect experiments, allowing collider results to be incorporated with other experimental searches in a complementary fashion [101]. However, it has been noted that caution must be exercised in naively applying the field theory approach at the LHC as well as in translating this to other search channels [102, 103].

Improve, and talk about a future collider and how it might help.

1.4.2 Indirect detection

FINISH THIS SECTION!

The possibility of dark matter annihilation into SM particles (as described in Fig. 1.3(b)) means that DM may be detected indirectly, by searching for these excess annihilation products (and related decay products). Some searches aim to look for the contribution of these products to signals obtained over large areas. The Fermi-LAT collaboration have published limits on searches for spectral lines and contributions to the diffuse background of gamma-rays [104]. Cosmic ray experiments such as PAMELA [105] **and ...** have aimed to measure the $p^{\pm}$ and $e^{\pm}$ abundances in cosmic rays. The AMS experiment [106] has recently reported a rise in the cosmic ray positron fraction at energies above 10 GeV, which has been interpreted as tentative evidence for dark matter annihilations (see e.g. Ref. [107] **and others**). In the case of charged particle cosmic rays, astrophysical magnetic fields deflect the paths of particles, meaning that it can be difficult to resolve individual sources [].

In contrast, photon searches allow specific locations to be targeted. Because the signal rate is proportional to the DM annihilation rate (along the line of sight), the potential signal scales as the square of the dark matter density. Thus, searching in areas where the DM density is expected to be high can boost the signal rate significantly [108]. As has already been discussed, dSph galaxies are dark matter dominated objects and thus represent promising targets for indirect searches. A survey of 25 Milky Way satellite galaxies by the Fermi-LAT telescope [109] has so far found no significant gamma-ray signal, however, again constraining the possible DM annihilation cross section *give values*. By optimising search regions near the centre of the Milky Way for maximum signal-to-noise, Weniger recently found a bump in the gamma-ray spectrum of Fermi-LAT data around 130 GeV [110]. However, subsequent analysis has found that this feature may be a systematic effect in the detector [111] and that it is difficult to reconcile with conventional models for dark matter [112, 113].

Perhaps more promising is a different gamma ray signal coming from the inner regions of the Galaxy, peaking at energies around 1-3 GeV [114, 115]. Fits of the data point towards a dark matter particle with a mass of 31-40

GeV, annihilating predominantly to $b\bar{b}$ with a cross section of $\langle\sigma v\rangle(1.4 - 2.0) \times 10^{-26}$ cm^3 s^{-1}, approximately matching the value required for a particle created by thermal freeze-out in the early universe. While it has been suggested that this signal is actually consistent with known sources [116] or as yet unresolved astrophysical sources [117], further analysis has shown that the signal matches the spectrum and morphology expected from DM annihilation [118]. **Mention the significance...** Confirmation of the signal may have to wait until it is corroborated by independent observations, for example a DM annihilation signal from dSph galaxies.

Another potentially rich source of DM annihilations are the Sun and Earth. DM particles may scatter with nuclei in these bodies, losing energy and eventually becoming captured. Eventually, the DM sinks to the centre of the object and annihilates. The only annihilation products which can escape are neutrinos which can then be detected at neutrino telescopes such as ANTARES [119] and IceCube [120]. Because the neutrino flux depends on the scattering rate of DM with nuclei, such signals can probe similar (but complementary) parameter spaces to direct detection experiments. We treat this subject in more detail in Chapter **??**.

Give some solid results and talk about future experiments.

ICECUBE SEARCHES FOR DM ANNIHILATION IN GALAXIES AND CLUSTERS [121]

IACTS: HESS, MAGIC, VERITAS and CTA [122]

1.4.3 Direct detection

Processes described by the diagram in Fig. 1.3(c) lead to the possibility of scattering between DM and SM particles. The principle of direct detection is to look for nuclear recoils due to this scattering in a dedicated detector [**?** **?**]. However, WIMPs with GeV-scale masses and speeds $v \sim 10^{-3}c$ (as predicted by N-body simulations [**?**] and direct calculations []) are expected to produce keV-scale nuclear recoils. In addition, due to the expected low cross section for such interactions, the predicted rate is less than around 1 event per year per kg of detector mass **Check and cite**. Detecting such rare, low energy recoils requires not only large ton-scale detectors, but also sophisticated methods for discriminating signal from background.

Write one paragraph about the tentative signals. Start with the refer-

ences in here arXiv:1207.2039. Go back and do this after I've done the DD chapter.

The interpretation of direct detection data will be the main focus of this work and we will therefore defer a more detailed discussion until Chapter **??**.

Say something about complementarity between these 3.

1.4.4 Conclusions

The ΛCDM paradigm has enjoyed great success in explaining observations from galactic to cosmological scales. While discrepancies with observations on smaller scales remain, these are being actively pursued and may prove to be valuable testing grounds for the process of dark matter structure formation. The identity of dark matter is unknown and cannot be accounted for by any of the known standard model particles. Even so, we know that it must be neutral, long-lived and cold (or possibly warm) and that it must pass a variety of stringent tests coming from BBN and the CMB. There is no lack of well-motivated CDM candidates, including the lightest supersymmetric and Kaluza-Klein particles, sterile neutrinos, axions and many more. We have focussed on the search for weakly interacting massive particles (WIMPs) and shown that tight limits have been set by a wide range of direct, indirect and collider experiments and that the prospects for detecting WIMPs in the near future are good.

Chapter 2

Direct detection of dark matter

2.1 Introduction

Definitely need to include a little bit about what the event rates actually look like. Some plots and stuff...

The idea that particle dark matter (DM) may be observed in terrestrial detectors was first proposed by Goodman and Witten in 1985 [123] and by Drukier, Freese and Spergel in 1986 [124]. If DM can interact with particles of the Standard Model, the flux of DM from the halo of the Milky Way should be large enough to cause measureable scattering from nuclei. If the subsequent recoils can be detected and their energy spectrum measured, it should be possible to infer some properties of the DM particles.

However, the expected event rate for keV-scale recoils at such a detector would be of the order of 10^{-10} events per kg of detector material per day per keV recoil energy [125]. With such a low event rate, it is imperative that backgrounds can be reduced as much as possible. In addition, detectors should be as large as possible and sensitive to as wide a range of recoil energies as possible, in order to maximise the total number of events observed. Thus, specialised detectors are required to shield the active detector material from backgrounds and to discriminate between these backgrounds and signal events.

There exist at present a wide range of detectors using a variety of different sophisticated techniques for detecting such a weak signal against ubiquitous backgrounds, each probing a slightly different range of DM pa-

rameter space. Several of these experiments - such as DAMA/LIBRA [126], CoGeNT [127, 128] and CRESST-II [129] - claim to have observed a signal indicative of a WIMP with mass $\sim$ 10 GeV. However, a number of other experiments have reported null results creating tension for a dark matter interpretation of these tentative signals. It remains to be seen whether this discrepancy is an experimental effect or physically meaningful result.

There remain a number of uncertainties in the direct detection of dark matter. These come from a variety of sources and can be approximately partitioned into experimental, nuclear, particle and astrophysical uncertainties. Understanding these uncertainties is imperative for properly interpreting the results of direct detection experiments and understanding whether a coherent picture can emerge from a number of different experimental efforts.

In this chapter, I will review the formalism for direct detection which was introduced by Goodman, Witten, Drukier, Freese and Spergel in the 1980s (and subsequently refined). I will then briefly discuss some of the experimental techniques which are used to achieve the required sensitivity for DM searches, as well as summarising current experimental constraints and results. I will outline some of the uncertainties which afflict the interpretation of direct detection data.

I will focus on astrophysical uncertainties in direct detection. In particular, I will discuss the local density and distribution of dark matter impacts the direct detection event rate, how well we understand these different factors and review approaches which have been developed in the past to mitigate these uncertainties.

2.2 Direct detection formalism

Make sure I get the right citations and stuff in here... Generalise to many nuclei etc... **Make the distinction NOW about f1 or f or f3 and what I mean by that...**

ELASTIC SCATTERING - what about the alternatives? Form factor DM, higher order stuff, effective operator, inelastic?

This only applies to fermionic dark matter!!!

Introduce the term WIMPs

We wish to obtain the rate of nuclear recoils per unit detector mass.

The differential event rate R can be written straightforwardly as

$$\frac{\mathrm{d}R}{\mathrm{d}E_R} = N_T \Phi_\chi \frac{\mathrm{d}\sigma}{\mathrm{d}E_R}\,, \tag{2.1}$$

for recoils of energy E_R, N_T target particles, a DM flux of Φ_χ and a differential scattering cross section of $\frac{\mathrm{d}\sigma}{\mathrm{d}E_R}$. Per unit detector mass, the number of target particles is simply $N_T = 1/m_N$, for nuclei of mass m_N. The DM flux for particles with speed in the range $v \to v + \mathrm{d}v$ is $\Phi_\chi = n_\chi v f(v)\,\mathrm{d}v$. Here, n_χ is the number density of dark matter particles χ and $f(v)$ is the speed distribution for the dark matter. This distribution function describes the fraction of DM particles having a given speed. Finally, we can convert from the number density to the mass density ρ_0 by dividing by DM particle mass m_χ: $n_\chi = \rho_0/m_\chi$. By integrating over all DM speeds, we therefore obtain

$$\frac{\mathrm{d}R}{\mathrm{d}E_R} = \frac{\rho_0}{m_N m_\chi} \int_{v_{\min}}^{\infty} v f(v) \frac{\mathrm{d}\sigma}{\mathrm{d}E_R}\,\mathrm{d}v\,, \tag{2.2}$$

where $v_{\min}$ is the minimum speed required to excite a nuclear recoil of energy E_R:

$$v_{\min} = \sqrt{\frac{m_N E_R}{2\mu_{\chi N}^2}}\,. \tag{2.3}$$

The differential scattering cross section per solid angle in the zero-momentum frame (ZMF), Ω^*, is given by:

$$\frac{\mathrm{d}\sigma}{\mathrm{d}\Omega^*} = \frac{1}{64\pi^2 s}\frac{p_f^*}{p_i^*}|\mathcal{M}|^2\,, \tag{2.4}$$

where $\mathcal{M}$ is the scattering amplitude obtained from the Lagrangian. For elastic scattering, the final and initial momenta in the ZMF are equal: $p_f^* = p_i^*$. The centre-of-mass energy squared, s, can be written $s \approx (m_\chi + m_N)^2$, where we have used the non-relativistic approximation **This is only justified later**. The recoil energy can be written in terms of the ZMF scattering angle θ^* as [125]

$$E_R = \frac{\mu_{\chi N}^2 v^2}{m_N}(1 - \cos\theta^*)\,. \tag{2.5}$$

Noting that $\mathrm{d}\Omega^* = \mathrm{d}\cos\theta^* \mathrm{d}\phi$, we can write:

$$\frac{\mathrm{d}E_R}{\mathrm{d}\Omega^*} = \frac{\mu_{\chi N}^2 v^2}{2\pi m_N}\,, \tag{2.6}$$

and therefore

$$\frac{\mathrm{d}\sigma}{\mathrm{d}E_R} = \frac{1}{32\pi m_N m_\chi^2 v^2}|\mathcal{M}|^2 \,. \tag{2.7}$$

The matrix element $\mathcal{M}$ is obtained from interaction terms in the lagrangian between the DM particle and quarks. This will depend on the particular DM model under consideration and the full form of these interaction terms is not known. However, because the WIMPs have speeds of order $10^{-3}c$, the scattering occurs in the non-relativistic limit, leading to some important simplifications. In this limit, the axial-vector interaction simply couples the spins of the WIMP and quark. The scalar interaction induces a coupling of the WIMP to the number of nucleons in the nucleus, with the vector[1] and tensor interactions assuming the same form as the scalar in the non-relativistic limit [74]. All other interactions are typically suppressed by powers of v/c and so will be subdominant (though we will consider briefly scenarios where this is not the case in Sec. **??**). **Check and cite...** Generically, then, the cross section is typically written in terms of spin-independent (SI) and spin-dependent (SD) interactions [123] **Talk a bit more here about effective field theories - find the right paper - there's one that has all the v/c dependences - mentioned in [130]... - only considering contact interactions, slow moving spin-1/2,...[131–134] - axial-vector and scalar currents do not interfere...**

$$\frac{\mathrm{d}\sigma}{\mathrm{d}E_R} = \frac{\mathrm{d}\sigma_{SI}}{\mathrm{d}E_R} + \frac{\mathrm{d}\sigma_{SD}}{\mathrm{d}E_R} \,. \tag{2.8}$$

We now discuss the form of the SI and SD cross sections in turn.

2.2.1 SI interactions

Spin-independent interactions are generated predominantly by scalar terms in the effective lagrangian**NB: Contact interactions in some effective field theory - what about loop diagrams...?**

Does the scalar couple to the number or the mass?

$$\mathcal{L} \supset \alpha_S^{(q)} \bar{\chi}\chi\bar{q}q \,, \tag{2.9}$$

[1]For the case of a Majorana fermion, the vector current vanishes and we need not consider it.

for interactions with a quark species q with coupling $\alpha_S^{(q)}$. The operator $\bar{q}q$ is simply the quark number operator, which couples to the quark density. However, we should recall that the quarks are in nucleon bound states $|n\rangle$, so we should evaluate $\langle n|\bar{q}q|n\rangle$, adding coherently the contributions from both valence and sea quarks. These matrix elements are obtained from chiral perturbation theory [135] or Lattice QCD [136]. These matrix elements can be parametrised in terms of their contribution to the nucleon mass in the form:

$$m_n f_{Tq}^n \equiv \langle n|m_q \bar{q}q|n\rangle \,. \tag{2.10}$$

Adding the contributions of the light quarks, as well as the heavy quarks and gluons (which contribute through the chiral anomaly [137]), we obtain

$$\langle n|\sum_{q,Q,g}\bar{q}q|n\rangle = \left(\sum_{q=u,d,s}\frac{m_n}{m_q}f_{Tq}^n\alpha_S^q + \frac{2}{27}f_{TQ}^n\sum_{q=c,b,t}\frac{m_n}{m_q}\alpha_S^q\right) \equiv f^n \,. \tag{2.11}$$

The parameters describing the contributions of the different quarks to the nucleon mass be determined experimentally. The uncertainties this produces will be discussed shortly in Sec. **??**. **Check - what exactly is this equal to...**

We now consider the matrix elements of the nucleon operators within a nuclear state, $|\Psi_N\rangle$:$\langle\Psi_N|f^n\bar{n}n|\Psi_N\rangle$. These operators now simply count the number of n nucleons in the nucleus, along with a momentum-dependent form factor, $F(\mathbf{q})$, corresponding to the Fourier transform of the nucleon density. This takes into account the loss of coherence for nuclear scattering due to the fact that the nucleus is not point-like. We therefore obtain:

$$\langle\Psi_N|f^n\bar{n}n|\Psi_N\rangle = \langle\Psi_N|\Psi_N\rangle f^n N_n F_n(\mathbf{q}) = 2m_N f^n N_n F_n(\mathbf{q}) \,, \tag{2.12}$$

where we note that we require the wavefunctions to be normalised to $2E \approx 2m_N$ for a nucleus of mass m_N. We now add the contribution from protons to the matrix element, noting that $F_n \approx F_p = F$ (see Sec. **??**)

$$\langle\Psi_N|f^n\bar{n}n + f^p\bar{p}p|\Psi_N\rangle = 2m_N(f^n N_n + f^p N_p)F(\mathbf{q}) \,, \tag{2.13}$$

where N_n and N_p are the neutron and proton numbers of the nucleus respectively.

The corresponding matrix element for the scalar WIMP operator $\bar{\chi}\chi$ is simple in the non-relativistic limit, evaluating to $2m_\chi$ []. Combining these,

we obtain the scalar matrix element

$$|\mathcal{M}_S|^2 = 16 m_\chi^2 m_N^2 \left| f^p Z + f^n (A - Z) \right|^2 F_{SI}^2(\mathbf{q}) \,, \tag{2.14}$$

and the SI cross section

$$\frac{\mathrm{d}\sigma_{SI}}{\mathrm{d}E_R} = \frac{m_N}{2\pi v^2} \left| f^p Z + f^n (A - Z) \right|^2 F^2(\mathbf{q}) \,, \tag{2.15}$$

where we have used the atomic number Z and mass number A to describe the composition of the nucleus. It is conventional to write this in terms of the **total** WIMP-proton SI cross section, which does not depend on the particular (A, Z) of the target nucleus and thus allows easy comparison between experiments. This cross section is given by

$$\sigma_{SI}^p = \frac{\mu_{\chi p}^2}{\pi} (f^p)^2 \,, \tag{2.16}$$

meaning that

$$\frac{\mathrm{d}\sigma_{SI}}{\mathrm{d}E_R} = \frac{m_N}{2\mu_{\chi p}^2 v^2} \left| Z + (f^n/f^p)(A - Z) \right|^2 F^2(E_R) \,. \tag{2.17}$$

TALK ABOUT fn/fp.

Talk about the vector contribution - subdominant

Mention spin 0 and spin 1

Distinguish between nucleon and neutron with n

2.2.2 SD interactions

The spin-dependent interaction is typically sourced by axial-vector currents of the form

$$\mathcal{L} \supset \alpha_{AV}^{(q)} (\bar{\chi} \gamma^\mu \gamma_5 \chi)(\bar{q} \gamma_\mu \gamma_5 q) \,. \tag{2.18}$$

These result in a coupling of the spins of the WIMP and nucleus. In analogy with the SI case, we can write the nucleon quark matrix elements in the form [130, 138]

$$\langle n | \bar{q} \gamma_\mu \gamma_5 q | n \rangle = 2 s_\mu^n \Delta_q^n \,, \tag{2.19}$$

where s_μ is the nucleon **/neutron** spin 4-vector and Δ_q^n parametrises the contribution of quark q to this total spin. Adding the contributions of the different quarks, we can define

$$a_{p,n} = \sum_{q=u,d,s} \frac{\alpha_{AV}^{(q)}}{\sqrt{2}G_F} \Delta_q^{p,n} \,, \tag{2.20}$$

which are the effective proton and neutron spin couplings.

The full nuclear matrix elements can then be written in the form

$$\langle \Psi_N | \sum_{q=u,d,s} \bar{q}\gamma_\mu\gamma_5 q | \Psi_N \rangle = 4\sqrt{2}G_F \frac{a_p\langle S_p\rangle + a_n\langle S_N\rangle}{J} \langle \Psi_N | \hat{J} | \Psi_N \rangle F_{SD}^2(E_R) \tag{2.21}$$

where J is the total nuclear spin, $\langle S_{p,n}\rangle$ the expectation value of the total proton and neutron spin in the nucleus and F_{SD}^2 is a form factor, as in the SI case, which is determined by the internal spin structure of the nucleus. **Should that be $4\sqrt{2}$ or $2\sqrt{2}$?** Noting that $\langle \Psi_N | \hat{J} | \Psi_N \rangle = 2J(J+1)m_N$, we obtain for the SD cross section

$$\frac{\mathrm{d}\sigma_{SD}}{\mathrm{d}E_R} = \frac{16 m_N}{\pi v^2} G_F^2 \frac{J+1}{J} \left| a_p\langle S_p\rangle + a_n\langle S_n\rangle \right|^2 F_{SD}^2(E_R) \,. \tag{2.22}$$

Say something about the form factor - and about the 'alternate' non-form factor version...Also what about the neutralino axial vector matrix element - is that just 2 mx?

Again, as in the SI case, it is convenient to rewrite this expression in terms of the proton cross section σ_{SD}^p, which is given by **be more explicit about how we obtain the cross section - i.e. using the $\frac{\mathrm{d}\sigma}{\mathrm{d}\Omega^*}$ equation...**

$$\sigma_{SD}^p = \frac{96}{4} G_F^2 \frac{\mu_{\chi p}^2}{\pi} (a_p)^2 \,. \tag{2.23}$$

This leads to the final expression for the SD cross section

$$\frac{\mathrm{d}\sigma_{SD}}{\mathrm{d}E_R} = \frac{2 m_N \sigma_{SD}^p}{3\mu_{\chi p}^2 v^2} \frac{J+1}{J} \left| \langle S_p\rangle + (a_n/a_p)\langle S_n\rangle \right|^2 F_{SD}^2(E_R) \,. \tag{2.24}$$

2.2.3 The final event rate

It is helpful to collect these various results together to form a coherent picture of the event rate. Combining the SI and SD rates together, we can write

$$\frac{\mathrm{d}\sigma}{\mathrm{d}E_R} = \frac{m_N}{2\mu_{\chi p}^2 v^2}\left(\sigma_{SI}^p \mathcal{C}_{SI} F_{SI}^2(E_R) + \sigma_{SD}^p \mathcal{C}_{SD} F_{SD}^2(E_R)\right) , \tag{2.25}$$

where the proton cross sections $\sigma_{SI,SD}^p$ were defined in the previous section, the form factors $F_{SI,SD}^2$ will be discussed in more detail in Sec. **??** and we have defined the enhancement factors as

$$\mathcal{C}_{SI} = |Z + (f^n/f^p)(A-Z)|^2 \tag{2.26}$$

$$\mathcal{C}_{SD} = \frac{4}{3}\frac{J+1}{J}\left|\langle S_p\rangle + (a_n/a_p)\langle S_n\rangle\right|^2 . \tag{2.27}$$

We can now incorporate these into the full event rate:

$$\frac{\mathrm{d}R}{\mathrm{d}E_R} = \frac{\rho_0}{2\mu_{\chi p}^2 m_x}\left(\sigma_{SI}^p \mathcal{C}_{SI} F_{SI}^2(E_R) + \sigma_{SD}^p \mathcal{C}_{SD} F_{SD}^2(E_R)\right)\int_{v_{\min}}^{\infty}\frac{f(v)}{v}\,\mathrm{d}v\,. \tag{2.28}$$

For a given experiment, which is sensitive to recoil energies in the range $E_{\min}$ to $E_{\max}$, the total number of events expected is obtained by integrating over this range of recoil energies and multiplying by the exposure time $t_{\exp}$, detector mass $m_{\det}$ and efficiency (which may also be a function of the recoil energy E_R) $\epsilon(E_R)$:

$$N_e = m_{\det} t_{\exp}\int_{E_{\min}}^{E_{\max}} \epsilon(E_R)\frac{\mathrm{d}R}{\mathrm{d}E_R}\,\mathrm{d}E_R\,. \tag{2.29}$$

For the case of a more realistic experiment in which the measurement of energy has only a finite resolution $\sigma(E_R)$, we convolve the event rate with a resolution function to obtain the observed recoil spectrum $\frac{\mathrm{d}\tilde{R}}{\mathrm{d}E_R}$,

$$\frac{\mathrm{d}\tilde{R}}{\mathrm{d}E_R}(E) = \int_{E'=0}^{\infty}\frac{\mathrm{e}^{-(E-E')^2/(2\sigma(E'))}}{\sqrt{2\pi}\sigma(E')}\frac{\mathrm{d}R}{\mathrm{d}E_R}(E')\,\mathrm{d}E'\,. \tag{2.30}$$

We now turn our attention to the discussion of such 'realistic experiments' and the current state of dark matter direct searches.

SI good for heavier detectors... Annual modulation Isospin conserving assumptions... *Add in some plots and discussion of event rates etc...*

2.3 Direct detection experiments

Typical sources of backgrounds include i) e/γ events, ii) neutrons, iii) α-particles and iv) nuclear recoils.

In order to measure this spectrum, a range of obstacles must be overcome. Radioactive decays due to naturally occuring isotopes may cause keV energy nuclear recoils in the detector, meaning that care must be taken to reduce their impact. The radiopurity of the target material is therefore of utmost importance (see for example Ref. [139]), as well as the radiopurity of detector equipment itself [140, 141] **Need clean construction...**. In some cases, the naturally occurring target material is contaminated with a particular radioisotope, such as ^{39}Ar contamination in Argon. In these cases, special sources of the material must be found [142], or the amount of contamination must be carefully measured and accounted for in data analysis [143] **I think they do actually remove the Krypton...**. **These are αs and γs I think...**

Exchange this paragraph with the one before... Another possible source of backgrounds are high energy cosmic rays. For this reason, direct detection experiments are typically operated underground, such as at the Gran Sasso laboratory in Italy or the Boulby laboratory in the UK, in order to reduce the penetration of these cosmic rays. However, cosmogenic neutrons can still penetrate the experiments, leading to the need for active shield which can detect these neutrons **and muons?** and provide a veto for any nuclear recoils they produce in the detector. Passive shielding also reduces the neutron flux from surrounding rock and other sources **environmental radioactivity**. For a detailed analysis of neutron sources at dark matter experiments, see Ref. [144] (CRESST-II) and Ref. [145] (XENON100).

Neutrons from U/Th contamination in the detector and surrounding materials; neutrons look exactly like WIMPs

Reject multiple events etc.; veto anti-coincident...

A major source of backgrounds is also electron recoils, which deposit energy in the detector and must be distinguished from nuclear recoils caused by WIMP interactions. Depending on the design of the detector, different methods are used to discriminate electron from nuclear recoils and to measure the recoil energy itself. We will now summarise some of the techniques which are used.

Use this list... *Say something about energy calibration and NR and*

EE... Which ones are sensitive to spin independent and spin dependent?

Cryogenic experiments, such as CDMS [146–148], CRESST [149], CoGeNT [127, 128, 150–152] and EDELWEISS [153], use cryogenic crystals of materials such as Germanium or Silicon as target materials. When a WIMP recoils from a target nucleus a phonon signal is generated in the crystal along with an ionization signal **be more technical - how are they measured**. By summing the energy collected in these two channels (and accounting for any which may be incompletely collected), the total energy of the nuclear recoil can be obtained. The ratio of the total nuclear recoil energy and the ionization signal is referred to as the 'ionisation yield' and can be used to discriminate electron from nuclear recoils; electron recoils deposit more energy into ionisation. However, care must be taken to identify so-called 'surface events' - events occurring close to the detector surface which result in an incomplete collection of ionisation signal and can thus mimic a WIMP signal.

Noble liquid experiments use liquid (or two-phase) noble elements such as Xenon and Argon as target materials. Completed or operational Xenon detectors include ZEPLIN [154], XENON [155] and LUX [156]. In these detectors, Xenon recoils produce a scintillation signal (S1) which can be observed directly using photomultiplier tubes. Ionisation electrons are also produced, which drift in an applied magnetic field, producing an electroluminescence signal (S2) in the gas phase. The sum of these signals can be used to reconstruct the total recoil energy, while the ratio S1/S2 is used to discriminate electron from nuclear recoils. **TPC** The two signals can also be used to localise the event within the detectors. A fiducial volume is then defined within the detector - only events inside this volume are considered in data analysis. This allows liquid Noble detectors to be self-shielding; the fiducial volume is shielded by the remaining detector volume. Experiments utilising Argon [157, 158] and Neon [159] are currently under development, using either the scintillation to ionisation signal as a discriminant or using timing of the scintillation signal (pulse shape discrimination).

Superheated liquid detectors such as COUPP [160], SIMPLE [161] and PICASSO [162] use a detector volume filled with droplets of superheated liquid such as C_4F_{10}. The deposition of kinetic energy by a WIMP will induce the nucleation of a bubble producing an acoustic signal which is detected by piezoelectric transducers. Energy deposition by other particles such as muons and γ- and β-radiation typically occurs over longer length

scales and thus does not register a signal. The temperature and pressure of the detector can be tuned to specify the threshold energy, the minimum energy which must be deposited before nucleation occurs. As such, superheated liquid detectors cannot measure the energy of specific events but rather the total event rate above the energy threshold. However, by ramping up the energy threshold, the recoil spectrum can effectively be measured. **Sensitive to SD and light WIMPs**.

Crystal scintillator experiments [163] such as DAMA/LIBRA [126, 164, 165] and KIMS [166] use crystals such as Thallium-doped Sodium Iodide (NaI(Tl)) as the detector material. When a nuclear recoil occurs with the nuclei in the crystal, scintillation occurs. The light is collected by photomultiplier tubes, with the total recoil energy being related to the amount of scintillation light produced. In the case of DAMA/LIBRA, electron-nuclear recoil discrimination is not employed. Instead, the experiment aims to observe the annual modulation of the signal which is expected due to the periodic motion of the Earth through the WIMP halo. In other cases, such as NAIAD [167], pulse shape discrimination has been used to distinguish nuclear and electronic recoils.

A final class of direct detection experiments are known as 'directional' direct detection experiments. These aim to measure not only the energy deposited by WIMP scattering events but also the direction of the nuclear recoils. **Why?** This requires the use of specialised gas time projection chambers (TPCs), which allow measurable track lengths from which the recoil direction can be determined. **Is any of this true?** The directional detection of dark matter is the subject of Chapter **??** and we therefore defer a more detailed discussion until then.

Neutrinos backgrounds...

2.3.1 Current limits and results

The first major dark matter detection to be reported was that of DAMA/NaI [168] and its successor DAMA/LIBRA. The experiments observed an annual modulation over 13 annual cycles, with a phase matching that expected from a dark matter signal. The detection of the annual modulation has been reported at the 8.9σ confidence level over an energy range of 2-6 keV. The modulation signal was only found in single-hit events at low energies, again suggesting a dark matter origin for the signal. Such a signal

is compatible with a wide range of particle physics scenarios [] and has been associated with a dark matter particle of mass $m_\chi \sim 10$ GeV and SI cross section $\sigma_{SI} \sim 10^{-41}$ cm^2 [169]. An annual modulation signal was also observed in the CoGeNT experiment [128, 151]. In this case too, the period and phase are consistent with expectations, though, in both cases the amplitude of the annual modulation is approximately 5 times larger than expected.

Excesses above the expected backgrounds have also been observed in a number of experiments.The CoGeNT experiment observed an exponentially rising excess of events at low energies, down to 0.5 keV$_{ee}$. A maximum likelihood analysis [152] pointed towards a 10 GeV WIMP interpretation, with a cross section of around $\sigma_{SI} \sim 5 \times 10^{-42}$ cm^2, though the significance of the 'signal' lies at only 2.9σ. CRESST-II observe 67 events in the nuclear recoil signal region but expect a background of only one event due to leakage of electron recoils into this window. Taking into account other backgrounds, the CRESST-II collaboration estimate that 25-30 of these events may be due to a WIMP signal. A fit to the data produces two minima in the likelihood function: one at $m_\chi \approx 25$ GeV (in which scattering from Tungsten is appreciable) and another at $m_\chi \approx 12$ GeV (where Tungsten recoils lie below the energy threshold). In both cases, the fitted cross section is in the range $\sigma_{SI} \approx 10^{-42} - 5 \times 10^{-41}$ cm^2. Finally, a recent analysis of the Silicon detector data from CDMS-II finds 3 events in the signal region. However, the very low expected backgrounds mean that this small number of events may be significant. The probability of the known backgrounds producing these three events has been calculated at 5.4% and a likelihood analysis shows consistency with WIMP with $m_\chi \approx 9$ GeV and $\sigma_{SI} \approx 2 \times 10^{-41}$ cm^2.

While it appears that a reasonably consistent picture of a low mass WIMP is emerging from several experiments [170], a large number of competing experiments have reported null results. Results from CDMS-II (Ge), XENON100, LUX, SuperCDMS [171] and others set upper limits on the standard WIMP cross section several orders of magnitude lower than the claimed signal. Several explanations for this discrepancy have been offered. One possibility is background contamination of the experiments claiming to have observed a signal [141]. Another possibility is that ion-channeling in the detector crystals may affect the collected ionisation signal and therefore alter the signal [172]. The DAMA/LIBRA signal has also been attributed

to an annually modulated muon signal [173, 174] or **WHAT ELSE?**.

An alternative explanation is that the claimed signals *are* due to a dark matter particle, but that its properties are not as simple as in the canonical case, explaining why it has not been observed in all experiments. One possibility is that the astrophysical distribution of dark matter does not match the standard assumptions. We will discuss this astrophysical distribution in more detail shortly in Sec. **??**. However, it appears that even with this additional freedom, the different results cannot be reconciled **Fairbairn:2009,Herrero-Garcia:2012,Fox:2011b,Frandsen:2012**. A number of particle physics models have also been considered to explain the results, including spin-dependent interactions [175], isospin violating dark matter (for which $f^p \neq f^n$) [176], inelastic dark matter [177] and mirror dark matter [178]. However, consistent picture which reconciles all experimental datasets remains elusive [179]. **IVDM is invoked to reduce sensitivity to a particular experiment...**

We summarise some of the completed and current direct detection experiments in Table 2.1. The most stringent limits on the SI WIMP-proton cross section are set by LUX [156], who find a limit of $\sigma^p_{SI} \leq 7.6 \times 10^{-46}$ cm^2 at a mass of $m_\chi = 33$ GeV. The best limit for the SD cross section is set by XENON100 [180]: $\sigma^p_{SD} \leq 3.5 \times 10^{-40}$ cm^2. The confirmation or falsification of the signals which have been claimed thus far may have to wait for the next generation of dark matter experiments, or for corroboration from collider or indirect searches.

More of the 'halo-independent' ones -Gondolo:2012,DelNobile:2013...

What about the halo-independent method?

Give some typical values for thresholds and efficiencies...

2.3.2 Future experiments

Experiments which are planned or under construction typically aim to scale up the size of current detectors and reduce unwanted backgrounds (in order to increase the sensitivity to lower cross sections) as well as decrease the energy threshold (which increases sensitivity to lower masses). There are a number of ton scale detectors either in operation or planned, including XENON1T [181], EURECA [182, 183] and DARWIN [184]. With this next generation of detectors, the aim is to achieve sensitivity to the SI WIMP-proton cross section down to $\sigma^p_{SI} = 10^{-48}$ cm^2.

Experiment	Target	Status
CDMS-II (Ge) [146, 147]	Ge	Null result
CDMS-II (Si) [148]	Si	Excess
SuperCDMS [171]	Ge	Null result
CoGeNT [127, 128, 150–152]	Ge	Excess & annual modulation observed
CRESST-II [149]	$CaWO_4$	Excess observed
EDELWEISS-II [153]	Ge	Null result
ZEPLIN-III [154]	Xe	Null result
XENON100 [155]	Xe	Null result
LUX [156]	Xe	Null result
PICASSO [162]	C_4F_{10}	Null result
SIMPLE-II [161]	C_2ClF_5	Null result
COUPP [160]	CF_3I	Null result
DAMA/LIBRA [126, 164, 165]	NaI(Tl)	Annual modulation observed
NAIAD [167]	NaI(Tl)	Null result
KIMS [166]	CsI(Tl)	Null result

Table 2.1: Summary of current and completed direct detection experiments.

In addition, there have been a number of proposals for novel methods of directly detecting dark matter. These include using DNA-based detectors to provide high spatial resolution [185], using nano-scale explosives [186] or charged-coupled devices [187] to achieve very low energy thresholds and using proton-beam experiments as a source for dark matter source for direct detection experiments [188].

Mini-conclusion...

What about electron recoils...?

2.4 Uncertainties

Calculation of the DM differential event rate $\frac{dR}{dE_R}$ requires not only a knowledge the dark matter parameters m_χ and $\sigma_{SI,SD}$ but a number of other factors which enter into the calculation. It is important to understand how uncertainties in these different factors and parameters propagates into the event rate in order to ensure that the conclusions we draw from direct detection experiments are unbiased. These uncertainties are typically partitioned into three separate classes: nuclear physics, particle physics and astrophysics.

2.4.1 Nuclear physics uncertainties

As we have already seen, nuclear physics enters into the calculation of the nucleon matrix elements $m_n f^n_{Tq} \equiv \langle n|m_q \bar{q} q|n\rangle$. The factors f^n_{Tq} must be determined experimentally, having values

$$f^p_{Tu} = 0.020 \pm 0.004; f^p_{Td} = 0.026 \pm 0.005; f^p_{Ts} = 0.118 \pm 0.062\,, \qquad (2.31)$$

with $f^p_{Tu} = f^n_{Td}$, $f^p_{Td} = f^n_{Tu}$ and $f^p_{Ts} = f^n_{Ts}$. **Strange content is most important - justifying fp = fn...?** The main uncertainties stem from determinations of the π-nucleon sigma term, determined either experimentally from low energy pion-nucleon scattering [135, 189, 190] or from lattice QCD calculations [136, 191]. Similarly for the spin contributions Δ_q to the nucleus, values must be obtained experimentally [130, 192–194], **Get up to date values...**

$$\Delta^p_u = 0.77 \pm 0.08; \Delta^p_d = -0.38 \pm 0.08; \Delta^p_s = -0.09 \pm 0.08\,, \qquad (2.32)$$

although efforts are being made to obtain these values directly via calculation [195, 196]. It should be noted that these nucleon matrix elements are only necessary if we wish to deal directly with quark-level couplings and interactions. If, instead, we consider the nucleon-level effective operators (and equivalently the WIMP-nucleon cross sections), these values are not required. **Is this from muon-proton scattering?**

Nuclear physics also enters into the calculation of form factors, describing the internal nucleon and spin structures of the nuclei. For the SI case, the form factor is obtained from the Fourier transform of the nucleon distribution in the nucleus. The form typically used is due to Helm [197]

$$F^2_{SI}(E_R) = \left(\frac{3j_1(qR_1)}{qR_1}\right)^2 \mathrm{e}^{-q^2 s^2}\,, \qquad (2.33)$$

where $j_1(x)$ is a spherical bessel function of the first kind,

$$j_1(x) = \frac{\sin x}{x^2} - \frac{\cos x}{x}\,. \qquad (2.34)$$

Typically used are nuclear parameters due to Lewin and Smith [198], based

on fits to muon spectroscopy data [199]:

$$R_1 = \sqrt{c^2 + \frac{7}{3}\pi^2 a^2 - 5s^2} \tag{2.35}$$

$$c = 1.23A^{1/3} - 0.60\text{fm} \tag{2.36}$$

$$a = 0.52\text{fm} \tag{2.37}$$

$$s = 0.9\text{fm}\,. \tag{2.38}$$

Muon spectroscopy is used as a probe of the *charge* distribution in the nucleus. However, detailed Hartree-Fock calculations indicate that the charge distribution can be used as a good proxy for the nucleon distribution (especially in the case $f_p \approx f_n$) and that using the approximate Helm form factor introduces an error of less than $\sim$5% in the total event rate [200]. Studies also indicate that errors due to distortions in nuclear shape away from sphericity are negligible [201].

Find that paper that compares all the different SI form factors...

Include a table of Sp and Sn values - or values for N, alpha, beta - table in [74] In the SD case, however, the situation is more complicated. In order to calculate the SD cross section, we require the proton and neutron spin content $\langle S_{p,n}\rangle$ as well as the form factor F^2_{SD}. The form factor can be written in the form

$$F^2_{SD}(E_R) = S(E_R)/S(0)\,, \tag{2.39}$$

in terms of the response function $S(E_R)$. This response function can in turn be decomposed into three spin-dependent structure functions (SDSFs)

$$S(E_R) = a_0^2 S_{00}(E_R) + a_0 a_1 S_{01}(E_R) + a_1^2 S_{11}(E_R)\,, \tag{2.40}$$

where $a_0 = a_p + a_n$ is the isoscalar coupling and $a_1 = a_p - a_n$ is the isovector coupling. The zero momentum transfer value $S(0)$ is related to the proton and neutron spin expectation values by [202]

$$S(0) = \frac{2J+1}{\pi}\frac{J+1}{J}\left|a_p\langle S_p\rangle + a_n\langle S_n\rangle\right|^2\,. \tag{2.41}$$

We can therefore rearrange the SD cross section of Eq. 2.24 as

$$\frac{\mathrm{d}\sigma_{SD}}{\mathrm{d}E_R} = \frac{2\pi}{3}\frac{m_N\sigma^p_{SD}}{\mu^2_{\chi p}v^2}\frac{1}{2J+1}\frac{S(E_R)}{(a_p)^2}\,. \tag{2.42}$$

The nuclear physics is now encapsulated in a single response function $S(E_R)$ (or equivalently two SDSFs S_{00} and S_{11}).[2]

The functional form for S_{ij} can be calculated from shell models for the nucleus [203]. However, there are a number of competing models (such as the Odd Group Model [204], Interacting Boson Fermion Model [205] and Independent Single Particle Shell Model [206] among others). These models use different methods for accounting for forces between quarks, leading to different forms for the SDSFs and therefore to significant uncertainty in the spin-dependent cross section. This issue was explored by Cerdeño et al. [207], who developed a parametrisation for the spin structure functions in terms of the parameter $u = (qb)^2/2$, where q is the momentum transfer and $b = \sqrt{41.467/(45.0A^{-1/3} - 25.0A^{-2/3})}$ is the oscillator size parameter. This parametrisation takes the form

$$S_{ij} = N((1-\beta)\mathrm{e}^{-\alpha u} + \beta)\,, \tag{2.43}$$

where the range of the parameters $\{N, \alpha, \beta\}$ is chosen such that S_{ij} spans the different possible forms presented in the literature. It was shown that this parametrisation was able to mitigate the uncertainties in the SD cross section and accurately recover the remaining particle physics parameters when the true form for the SDSFs was unknown.

2.4.2 Particle physics uncertainties

Apart from the unknown values for the WIMP mass m_χ and cross sections $\sigma_{SI,SD}$, the ratios of proton to neutron couplings are also *a priori* unknown. In the case of SI scattering, the dominant contribution comes from the coupling to strange quarks f_{Ts}, which is equal for protons and neutrons. It is therefore typically assumed that $f^p \approx f^n$, though as we have seen isospin violating dark matter models have been considered [176, 208, 209]. Similarly, for the SD interaction, a specific relation is typically assumed between the proton and neutron couplings, such as $a_p/a_n \approx \pm 1$. While specific models often predict such a relation [], it should be noted that this ratio is *a priori* unknown and fixing it is a model choice.

Further uncertainty is derived from the form of the interaction terms themselves. Here, we have considered the dominant contributions to scat-

[2] In Ref. [202], it is noted that the SDSFs are not independent and that the function S_{01} can be written in terms of the other two.

tering in the case of non-relativistic contact interactions. Extensions including mediator particles have been considered [210, 211], as well as models in which DM can interact electromagnetically with nuclei [212, 213]. There has also been significant effort towards developing a general non-relativistic field theory for the interaction of WIMPs with nuclei [131–134]. Current limits can be translated into limits on the couplings associated with a range of effective operators. While this approach significantly widens the parameter space of dark matter direct detection, it is more general and does not rely on (potentially poor) assumptions about DM interactions.

Asymmetric DM?

2.4.3 Astrophysical uncertainties

Astrophysical uncertainties enter into the direct detection event rate through the local dark matter density ρ_0 and the speed distribution $f(v)$.

DM density, ρ_0

The DM mass density sets the overall scale of the scattering rate. As we shall discuss in Chapter **??**, the DM density is degenerate with the interaction cross section, meaning that an accurate determination is important. One method of obtaining the value of ρ_0 is by mass modelling of the Milky Way (MW). One builds a model for the Galaxy incorporating various sources of mass, including the stellar bulge and disc, dust and a dark matter halo [214]. It is then possible to use various data such as the total MW mass, local surface mass density and the velocities of tracers **[some citations?]** to fit the parameters of this model and thereby extract ρ_0. Estimates using this method tend to have a wide uncertainty, typically lying in the range $0.2 - 0.4$ GeV cm^{-3} (e.g. Ref. [214, 215]). A more recent determination using state-of-the-art data obtains a more precise but higher value of $\rho_0 = 0.47^{0.05}_{-0.06}$ GeV cm^{-3} [216] (though this depends on the choice of halo density profile).

An alternative method is to use local stellar kinematic data to constrain the gravitational potential near the Sun and thus obtain an estimate of ρ_0. Using kinematic data from roughly 2000 K-dwarfs, Garbari et al. [217] obtain the value $\rho_0 = 0.85^{+0.57}_{-0.50}$ GeV cm^{-3} while Zhang et al. , using a larger sample of 9000 K-dwarfs, obtain 0.28 ± 0.08 GeV cm^{-3}. Including microlensing data, the range of allowed values at 1σ is $\rho_0 =$

$0.20 - 0.56$ GeV cm^{-3} [218]. The advantage of such approaches is that one does not need to assume a particular form for the DM halo density profile. However, they may be more sensitive to assumptions about local equilibrium near the Sun's position.

In 2012, Moni Bidin et al. [219] used the dynamics of thick disk stars to constrain the DM density, finding a result consistent with no dark matter at the Sun's radius. However, a subsequent reanalysis by Bovy and Tremaine [220] showed that this result derived from a poor assumption about the velocity of stellar tracers as a function of galactic radius. Using the same data with more reasonable assumptions, the value 0.3 ± 0.1 GeV cm^{-3} was obtained.

In spite of the large number of determinations, no consistent value appears to be emerging, with values ranging from $0.2-0.85$ GeV cm^{-3}. There also remain a number of uncertainties in these determinations, including the shape of the DM halo [] and assumptions about the local equilibrium of the Galaxy []. **Need citations**. The 'standard' value assumed in the analysis of direct detection experiments is 0.3 GeV cm^{-3}, though the exact origin of this number is unclear [221]. As we shall discuss in Chapter **??**, the DM density is

Could also include Salucci et al. [222]...

Talk about ultra-local distribution...

Speed distribution, $f(v)$

The speed distribution enters into the direct detection rate in the integral,

$$\eta(v_{\rm min}) \equiv \int_{v_{\rm min}}^{\infty} \frac{f(v)}{v}\, {\rm d}v\,, \tag{2.44}$$

which is referred to as the 'velocity integral' or the 'mean inverse speed.' Direct detection experiments are traditionally analyzed within the framework of the Standard Halo Model (SHM), in which WIMPs are assumed to have a Maxwell-Boltzmann speed distribution in the Galactic frame. **What about Earth/Sun motion and time dependence?** In the Earth's frame, this takes the form

$$f_{\rm SHM}(\mathbf{v}) = N \exp\left(-\frac{(\mathbf{v}-\mathbf{v}_{\rm lag})^2}{2\sigma_v^2}\right) \Theta(v_{\rm esc} - |\mathbf{v}-\mathbf{v}_{\rm lag}|)\,, \tag{2.45}$$

where $\mathbf{v}_{\rm lag}$ specifies the velocity of the Earth frame with respect to the local standard of rest (LSR) and σ_v the velocity dispersion. We truncate the distribution above the escape speed $v_{\rm esc}$ in the Galactic frame and the factor N is required to satisfy the normalization condition (Eq. **??**). **Distinguish between the velocity and speed distributions and write down the integrated form.** The SHM distribution is obtained assuming a spherical, isothermal DM halo with density profile $\rho \sim r^{-2}$ and results in the relation $\sigma_v = \sqrt{2}v_{\rm lag}$. **Need to be careful and sensible about notation here and check factors of sqrt, as well as finding a few citations...**

Within the SHM, there is some uncertainty on the parameters describing $f(v)$. The parameter $v_{\rm lag}$ is given by the local circular speed of the Sun $v_c = 218 \pm 7\,{\rm km\ s^{-1}}$ [223, 224] (plus a contribution from the Earth's motion relative to the Sun **...**). The galactic escape velocity can be estimated from the radial velocities of MW stars; the RAVE survey obtain the range $v_{\rm esc} = 533^{+54}_{-41}\,{\rm km\ s^{-1}}$ at 90% confidence [225, 226]. **MENTION THE EARTH'S MOTION...and finish this paragraph...** Moreover, it is not known how well the relation $\sigma_v = \sqrt{2}v_{\rm lag}$ holds **why?**, meaning that σ_v is in reality poorly constrained.

However, the SHM is unlikely to be an accurate representation of the DM halo - observations and N-body simulations indicate that the halo should deviate from a $1/r^2$ profile and may not be spherically symmetric. As a result alternative models have been proposed. Speed distributions associated with triaxial halos [227] or with more realistic density profiles [228] have been suggested, as well as analytic parametrisations which should provide more realistic behaviour at low and high speeds [229]. **Fix this last sentence, and talk more about Lisanti.** Self-consistent distribution functions reconstructed from the potential of the Milky Way have also been obtained [230, 231].

It is also possible to extract the speed distribution from N-body simulations. Such distribution functions tend [232–234] to peak at lower speeds than the SHM and have a more populated high speed tail. There are also indications that DM substructure may be significant, causing 'bumps' in the speed distribution, or that DM which has not completely phase-mixed - so-called 'debris flows' - may have a contribution [235]. **Show a plot** It should be noted that N-body simulations do not probe down to the sub-milliparsec scales which are probed by direct detection experiments. This means that N-body speed distributions are averaged over large volumes in

order to obtain sufficient statistics. The effect of probing the speed distribution over such large length scales (rather than on the ultra local scale of experiments) is not known. **talk about 'smoothing' effect of going to the Earth frame.**

Another result obtained from N-body simulations is the possibility of a dark disk. When baryons are included in simulations of galaxy formation, this results in the tidal distruption of DM subhaloes which are then preferentially dragged into the disk plane [236, 237]. The resulting dark disk corotates with approximately the same speed as the baryonic matter, though with a smaller velocity dispersion $\sigma_v^{DD} \sim 50\,\mathrm{km\ s^{-1}}$. This dark disk is expected to contribute an additional density 0.2-1.0 times the density of the halo (depending on the merger history of the Milky Way). The more recent ERIS results [24], comparing hydrodynamic and DM-only simulations, indicate a smaller density of just 10% that of the DM halo in a Milky Way mass galaxy.

Talk about ultra local distribution - and possibility of streams...

In Fig. **??**, we show some examples of possible dark matter speed distributions. **How does that relate to the rate...? Do plots of η...** These different distributions result in different event rates **as shown in PLOT**. The impact of uncertainties in the WIMP speed distribution has been much studied (see e.g. Refs. [238–240]) and it has been shown that poor assumptions about the speed distribution may result in biased reconstructions of the DM mass and cross sections from future direct detection data. **[Maybe make this part of my first 'results' chapter]** It is unknown which, if any, of these distributions best describes the true galactic DM speed distribution and there have therefore been numerous attempts to mitigate these uncertainties.

A first step is to extend the SHM to incorporate uncertainties in v_{lag}, σ_v and v_{esc} into reconstructions. Strigari and Trotta [241] introduce a simple model of the Milky Way mass distribution, from which SHM velocity parameters can be derived. They then use projected stellar kinematics and direct detection data to fit both the model parameters and the dark matter properties. A more direct approach is to directly fit the SHM velocity parameters, incorporating their uncertainties into the fitting likelihood. This method has been considered by Peter [242], and is typically used as a simple model of astrophysical uncertainties (especially in studies which focus on other aspects of direct detection, e.g. Ref. [243]). These methods

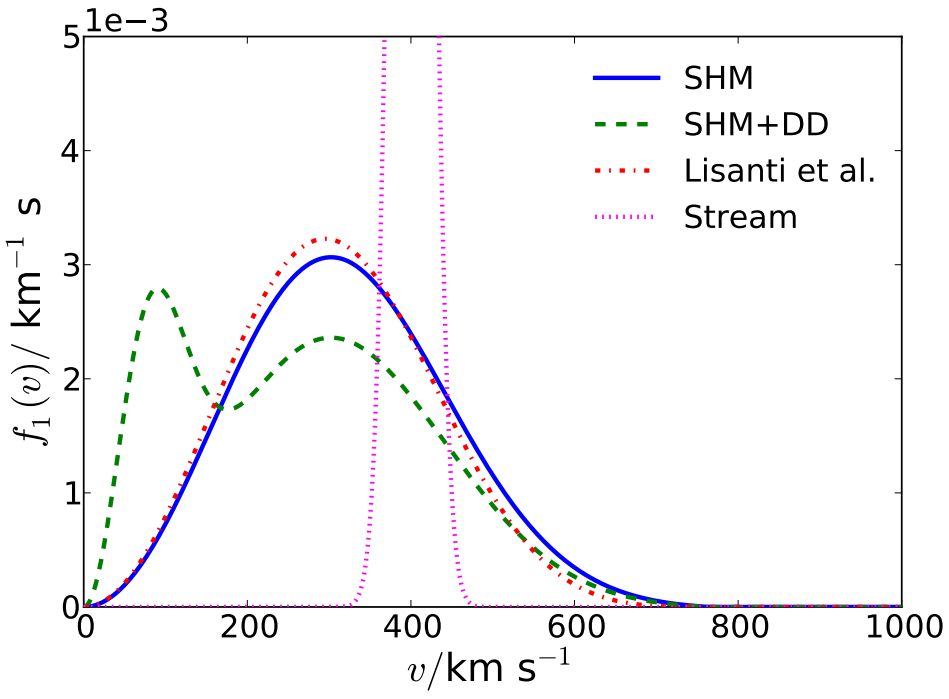

Figure 2.1: **Need actual caption - also, redo this plot.**

allow bias in the reconstructed WIMP parameters to be eliminated when the underlying speed distribution is indeed in the SHM form. However, as shown by Peter [239], these methods fail when the distribution function differs from the standard Maxwellian case.

There have also been attempts to incorporate and fit more realistic distribution functions. Pato et al. [244] incorporate astrophysical uncertainties by using the distribution function of Lisanti et al. [229] and fitting the various shape parameters associated with it. In a more recent paper, Pato et al. [245] use projected direct detection data to fit a model of the Milky Way mass distribution, from which they derive a self-consistent distribution function (SCDF) using Eddington's formula. This means that the resulting speed distribution will be consistent with the underlying potentials of the galaxy's bulge, disk and dark matter, incorporating a broader range of shapes than the SHM alone. However, as the authors point out, velocity distributions from cosmological N-body simulations differ significantly from those expected from Eddington's formula. As with the Standard Halo Model, fitting a realistically-motivated distribution function is likely to result in biased reconstructions if the true distribution deviates significantly

from the functional form used for fitting.

Methods which make no assumptions about the functional form of the speed distribution have had mixed success. Drees and Shan [246, 247] developed a method for estimating the WIMP mass by calculating moments of the speed distribution. However, this method still introduces a bias into the reconstructed WIMP mass and performs more poorly for heavier WIMPs and when finite energy thresholds are considered. An empirical ansatz for the speed distribution has also been suggested, specifically dividing the WIMP speed into a series of bins, with the distribution being constant within each bin [239]. **We will discuss this method in more detail in a later chapter...** However, both of these still result in a significant bias in the reconstructed mass and cross section. A recent proposal by Feldstein and Kahlhoefer [248] is to fit the velocity *integral* rather than the speed distribution. This proposal is the most promising so far and appears to give an unbiased reconstruction of the mass, though reconstructing the speed distribution itself remains problematic. **This is shit - I need to say something more concrete about these...**

Finally, a method for analysing existing data has been developed by various authors [249–251]. At a given mass, a given experiment is sensitive only to speeds in a fixed range, set by $v_{\rm min}(E_{\rm min})$ and $v_{\rm min}(E_{\rm max})$. By considering only the range of speeds where two or more experiments overlap, one can ensure that the astrophysical contribution to both experiments is equal. This method has typically been used to assess the compatibility of different data sets and to set more robust limits on the WIMP interaction cross sections. Recently it has also been extended to accomodate more general forms for the WIMP interactions [252]. **Again, be more specific - actually read these papers and put in some more detail - if it has to spill over into another chapter then fine... - Not sure, which is the McCabe one...**

Need to spend lots more time on this section - less time on other sections... - maybe send some of the detector stuff to the first chapter...or some of this stuff to a later chapter...

May even be able to reconstruct f(v) itself - why is that good?

Masses and which bits are probed by which...

2.5 Conclusion

We have discussed the dark matter direct detection formalism, focussing on the contribution from scalar and axial-vector contact interactions. The non-relativistic speeds involved means that the event rate can be divided into a spin-dependent and spin-independent contribution. A number of sophisticated experiments have been and continue to be developed which should allow these rare nuclear recoils to be detected. The use of different channels such as scintillation, ionisation and phonons not only allows the energy of these events to be measured but also allows discrimination against electronic recoils which can act as a significant background.

Tentative hints of a signal from the DAMA/LIBRA, CRESST-II and CoGeNT experiments have been interpreted as evidence for a WIMP with mass $m_\chi \sim 10$ GeV and cross section $\sigma_{SI} \sim 10^{-41}$ cm^2. However, null results from XENON, CDMS and other experiments are in tensions with this claimed signal. The origin of this discrepancy may lie in unidentified backgrounds or in an unconventional model for DM; corroboration from indirect and collider experiments may be needed before such a signal can be confirmed.

Finally, there are a number of uncertainties associated with calculating direct detection event rates and therefore with interpreting data from these experiments. Nuclear uncertainties are typically more important for SD rate than for the SI, though the method of Cerdeño et al. may be able to reduce the impact of such uncertainties. Particle physics uncertainties are significant, though the standard contact operator approach should be a good first approximation and effective field theories extending beyond this standard approach are being developed. Uncertainties in the *number* of dark matter particles, embodied in the local DM density ρ_0, lead to a factor of roughly 2 uncertainty in the total direct detection rate.

In contrast, uncertainties in the speed distribution of dark matter are poorly controlled. Theoretical and computational considerations indicate that the benchmark assumption - the SHM - is not a good description of the WIMP distribution and while a large number of alternatives are available, it is unclear which, if any, of these may be correct. Attempts to treat the speed distribution more generally in data analysis have had mixed success, either leading to a biased reconstruction of the WIMP parameters or requiring additional assumptions or information about the WIMP, such as its

mass. The wide range of possibilities for $f(v)$, as well as the consequences for misinterpreting future data, indicate that a more generalised approach is required.

Chapter 3

Parameter Reconstruction

3.1 Introduction

A common problem in physics is attempting to reconstruct the parameters of a model from a set of data. Stated more precisely, this is an attempt to answer the following question: given a set of data $\mathcal{D}$, what is the probability of a given set of model parameters $\boldsymbol{\theta}$ being the true, underlying parameters? But how do we interpret this question and what do we mean by the 'probability' of a given set of parameters?

In general, there are two approaches to parameter estimation. In *frequentist* inference, there is only a single, fixed set of true values for the model parameters $\boldsymbol{\theta}$. We imagine that the experiment (which produced the data $\mathcal{D}$) can be repeated a large number of times, giving independent results each time. The 'probability' associated with each set of parameters $\boldsymbol{\theta}$ is a measure of how frequently our experiment would produce data which looked similar to $\mathcal{D}$ if $\boldsymbol{\theta}$ is the true value. In a frequentist framework, the true model parameters are fixed but unknown and we make statements about how confident we are that these true parameters lie in a particular range.

An alternative approach is *Bayesian* inference. The true parameter value is treated as a random variable and we use Bayes theorem to determine its probability distribution from the data:

$$P(\boldsymbol{\theta}|\mathcal{D}) = P(\boldsymbol{\theta})\frac{P(\mathcal{D}|\boldsymbol{\theta})}{P(\mathcal{D})}\,. \tag{3.1}$$

In doing so, we need to know $P(\boldsymbol{\theta})$, known as the prior on the model parameters. This is a measure of our beliefs about the true value of $\boldsymbol{\theta}$ and

must be put in 'by hand'. In a Bayesian framework, we combine the data with information about our prior expectations to make statements about the probability of $\boldsymbol{\theta}$ having a particular value.

These two approaches have different strengths and weaknesses, as we shall explore, and have both been applied to the problem of parameter exploration in physics. In this chapter, we will discuss how both frequentist and Bayesian statistics are used to make parameter estimates and measure the degree of certainty in these estimates. We will describe several methods which are used to explore parameter spaces and therefore make parameter inferences. Finally, we will outline how to calculate the likelihood $\mathcal{L}$ - the probability of obtaining a particular set of data given some underlying model parameters - which is at the core of both the frequentist and Bayesian approaches.

3.2 Posterior distribution

Using the above techniques, we can obtain an estimate of the posterior distribution, or likelihood, for the N model parameters $\mathcal{L}(\mathbf{D}|\{\theta_i\})$.

It is sometimes necessary to calculate or plot the posterior distribution as a function of only a subset of parameters - say 1 or 2. While the full N-dimensional likelihood is unambiguous, the likelihood as a function of 1 or 2 parameters can be obtained in several ways, each of which encode different information. We discuss some of these ways below for the case of constructing a k-dimensional likelihood from the full N-dimensional parameter space.

Profile likelihood (PL) The profile likelihood is obtained by taking a k-dimensional slice of the full N-D likelihood. The choice of slice is somewhat arbitrary, but typically we choose to maximise the likelihood along the $N-k$ remaining dimensions:

$$\mathcal{L}_{\mathrm{PL}}(\theta_1, \theta_2, ..., \theta_k) = \max_{k+1,...,N} \mathcal{L}(\theta_1, \theta_2, ..., \theta_k, \theta_{k+1}, ..., \theta_N)\,. \tag{3.2}$$

Marginalised posterior The marginalised likelihood, or marginalised posterior, $\mathcal{L}_{\mathrm{M}}$ is obtained by integrating the full likelihood over the remaining $N-k$ dimensions.

$$\mathcal{L}_{\mathrm{M}}(\theta_1, \theta_2, ..., \theta_k) = \int \mathcal{L}(\theta_1, \theta_2, ..., \theta_k, \theta_{k+1}, ..., \theta_N)\,\mathrm{d}\theta_{k+1}...\mathrm{d}\theta_N\,. \tag{3.3}$$

3.3 Parameter estimates

While the entire posterior distribution is required to assess the fit of a single point, it can be helpful to report as single value for a given parameter as a measure of the location of the distribution. As before, reduction from one to zero dimensions can be ambiguous and we describe several possible options below.

Best fit The best fit parameter, or maximum likelihood estimator, is the parameter value which gives the largest likelihood over the entire parameter range.

Do the likelihoods for various things in here as well...poisson likelihood etc.

Chapter 4

Parametrising the dark matter momentum distribution

Chapter 5

A novel method for parametrising the speed distribution

Chapter 6

Breaking the cross section degeneracy: neutrino telescopes

Chapter 7

Speed parametrisation for directional experiments

7.1 Introduction

While traditional direct detection experiments seek to measure the recoil energies deposited by WIMPs scattering off detector nuclei, *directional* experiments aim to measure both the energy and direction of the recoil. While the recoil distribution of typical backgrounds is expected to be roughly isotropic, the WIMP-induced recoil distribution is expected to be highly directional. The motion of the Sun through the Galactic DM halo generates a so-called 'WIMP wind,' leading to an event rate peaked in the opposing direction, the direction of the constellation of Cygnus.

The ability of directional detection to distinguish background from signal and to provide a model independent confirmation of the dark matter origin of the signal make it a promising search strategy. However, measuring the direction of rare, low energy recoils remains challenging []. A number of directional detectors are currently in development and a number of novel methods for directional detection have been proposed.

Measuring the directional recoil spectrum allows us to probe not only the energy distribution of WIMPs in the Galactic halo (embodied in the speed distribution $f(v)$), but the full 3-dimensional velocity distribution $f(\mathbf{v})$. This may allow us to gain new insight into the formation processes at hand in the growth of the Milky Way halo []. However, it also introduces new uncertainty into calculating the event rate. While non-directional detection leaves us with a single free function in the form of $f(v)$, the direc-

tional case relies upon the *a priori* unknown function of a 3-dimensional vector, $f(\mathbf{v})$.

In this chapter, we will first introduce the formalism by which the directional rate is calculated. Specifically, we introduce the Radon transform which relates the WIMP velocity distribution to the corresponding nuclear recoil distribution. We then discuss the current state of directional detection technology and the progress of several directional experiments. We then discuss previous approaches to mitigating the uncertainties associated with the velocity distribution. Finally, we consider a new method for parametrising $f(\mathbf{v})$, which allows it to be written in terms of a finite number of one-dimensional functions, and how to calculate the Radon transform of this new, discretised distribution function.

7.2 Directional event rate

First, we wish to calculate the directional event spectrum in a dark matter detector. We follow the treatment of Gondolo [253], noting that similar calculations were performed previously by Copi, Heo and Krauss [254] and later by Copi and Krauss [255]. The scattering of a dark matter (DM) particle with a nucleus is illustrated in Fig. 7.1.

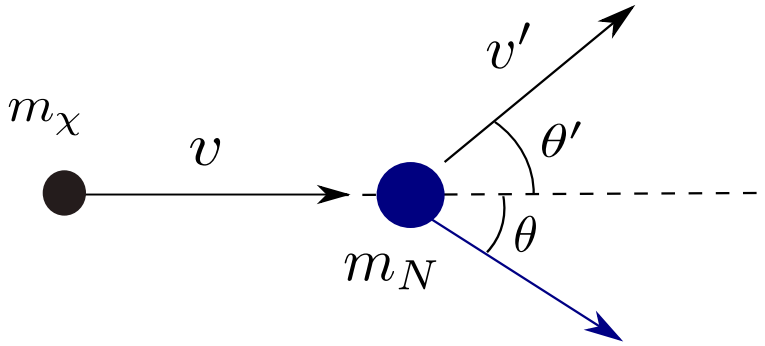

Figure 7.1: Illustration of the scattering of a DM particle of mass m_χ from a nucleus of mass m_N.

We consider a DM particle of mass m_χ impinging with velocity $\mathbf{v} = v\,(1, 0)$ on a stationary target nucleus of mass m_N. The dark matter scatters with velocity $\mathbf{v}' = v'\,(\cos\theta', \sin\theta')$ and the nucleus scatters with final momentum $\mathbf{q} = q\,(\cos\theta, \sin\theta)$. From conservation of linear momentum we obtain:

$$m_\chi v' \cos\theta' = m_\chi v - q\cos\theta\,, \tag{7.1}$$

$$m_\chi v' \sin\theta' = q\sin\theta\,. \tag{7.2}$$

We can eliminate θ' by summing the squares of Eqs. 7.1 and 7.2, to obtain:

$$v'^2 = v^2 - \frac{2vq\cos\theta}{m_\chi} + \frac{q^2}{m_\chi^2}\,. \tag{7.3}$$

From energy conservation, we obtain:

$$v'^2 = v^2 - \frac{q^2}{m_\chi m_N}\,. \tag{7.4}$$

Combining these, we see that the recoil momentum of the target nucleus is given by

$$q = 2\mu_{\chi N} v\cos\theta\,, \tag{7.5}$$

where $\mu_{\chi N} = m_\chi m_N/(m_\chi + m_N)$ is the DM-nucleus reduced mass.

For a WIMP-nucleus interaction cross section which is independent of velocity, we can write the differential cross section as

$$\frac{\mathrm{d}\sigma}{\mathrm{d}E_R} = \frac{m_N\sigma_p}{2\mu_{\chi p}^2 v^2}\mathcal{C}F^2(E_R)\,, \tag{7.6}$$

where E_R is the nuclear recoil energy, σ_p is the WIMP-proton interaction cross section (which may be spin-dependent (SD) or spin-independent (SI)) and $\mathcal{C}$ and F^2 are the corresponding enhancement factor and nuclear form factor (see Eq. 2.25).

We now obtain from here the double differential cross-section $\frac{\mathrm{d}\sigma}{\mathrm{d}E_R\mathrm{d}\Omega_q}$. The collision is azimuthally symmetric, so that $\mathrm{d}\Omega_q = 2\pi\,\mathrm{d}\cos\theta$. We then require a Dirac δ-function to impose the condition in Eq. 7.5: $\delta\left(\cos\theta - q/2\mu_{\chi N}v\right) = v\delta\left(v\cos\theta - q/2\mu_{\chi N}\right)$. We finally obtain

$$\frac{\mathrm{d}\sigma}{\mathrm{d}E_R\mathrm{d}\Omega_q} = \frac{m_N\sigma_p}{4\pi\mu_{\chi p}^2 v}\mathcal{C}F^2(E_R)\delta\left(v\cos\theta - v_{\min}\right) \tag{7.7}$$

where $v_{\min}$ is the minimum WIMP speed required to excite a recoil of momentum q or, equivalently, energy E_R:

$$v_{\min} = \frac{q}{2\mu_{\chi N}} = \sqrt{\frac{m_N E_R}{2\mu_{\chi N}^2}}\,. \tag{7.8}$$

To obtain the differential rate per unit detector mass, we divide by the mass of the target nucleus and multiply by the WIMP flux at velocity $\mathbf{v}$,

$$\frac{\rho_0}{m_\chi} v f(\mathbf{v})\, \mathrm{d}^3\mathbf{v}\,, \tag{7.9}$$

before integrating over all WIMP velocities, where ρ_0 is the local dark matter mass density. Combining these, we obtain:

$$\frac{\mathrm{d}R}{\mathrm{d}E_R \mathrm{d}\Omega_q} = \frac{\rho_0 \sigma_p}{4\pi \mu_{\chi p}^2 m_\chi} \mathcal{C} F^2(E_R) \hat{f}\left(v_{\min}, \hat{\mathbf{q}}\right)\,, \tag{7.10}$$

where $\hat{f}\left(v_{\min}, \hat{\mathbf{q}}\right)$ is the Radon Transform of the velocity distribution, defined as:

$$\hat{f}\left(v_{\min}, \hat{\mathbf{q}}\right) = \int \delta\left(v_{\min} - \mathbf{v}\cdot\hat{\mathbf{q}}\right) f(\mathbf{v})\, \mathrm{d}^3\mathbf{v}\,. \tag{7.11}$$

Geometrically, this is the integral of $f(\mathbf{v})$ over a plane perpendicular to $\hat{\mathbf{q}}$ at a distance $v_{\min}$ from the origin. In physical terms, for a given recoil angle and energy, we integrate over all WIMP velocities satisfying the kinematic constraint given by Eq. 7.5.

7.2.1 Examples

We consider several examples of velocity distributions and their corresponding Radon transforms. For an isotropic Maxwell-Boltzmann distribution with dispersion σ_v,

$$f(\mathbf{v}) = \frac{1}{\left(2\pi\sigma_v^2\right)^{\frac{3}{2}}} \exp\left[-\frac{\mathbf{v}^2}{2\sigma_v^2}\right]\,, \tag{7.12}$$

the Radon transform is also isotropic,

$$\hat{f}(v_q, \hat{\mathbf{q}}) = \frac{1}{\left(2\pi\sigma_v^2\right)^{\frac{1}{2}}} \exp\left[-\frac{v_q^2}{2\sigma_v^2}\right]\,. \tag{7.13}$$

If we take this form to describe the DM velocity distribution in the galactic frame, we must transform to the laboratory frame using the relation [253]

$$\hat{f}_{\mathrm{lab}}(v_q, \hat{\mathbf{q}}) = \hat{f}_{\mathrm{gal}}(v_q - \mathbf{v}_{\mathrm{lag}}\cdot\hat{\mathbf{q}}, \hat{\mathbf{q}})\,, \tag{7.14}$$

where $\mathbf{v}_{\rm lag}$ is the velocity of the peak of the galactic distribution with respect to the laboratory. We therefore obtain the Radon transform of the Standard Halo Model

$$\hat{f}(v_q, \hat{\mathbf{q}}) = \frac{1}{(2\pi\sigma_v^2)^{\frac{1}{2}}} \exp\left[-\frac{(v_q - \mathbf{v}_{\rm lag}\cdot\hat{\mathbf{q}})^2}{2\sigma_v^2}\right] . \tag{7.15}$$

This can be extended to incorporate a cut off at the galactic escape velocity, or for more general anisotropic velocity distributions [253].

Another interesting velocity distribution is that of a stream

$$f(\mathbf{v}) = \delta(\mathbf{v} - \mathbf{v}_s) , \tag{7.16}$$

which has Radon transform

$$\hat{f}(v_q, \hat{\mathbf{q}}) = \delta(v_q - \mathbf{v}_{\rm lag}\cdot\hat{\mathbf{q}}) . \tag{7.17}$$

This results in a highly directional signal, producing a spherical recoil spectrum centred on $\mathbf{v} = \mathbf{v}_s/2$.

In Fig. 7.2, we illustrate the Radon transform of the SHM (top), the SHM with a contribution from a dark disk (middle), and a stream (bottom). We evaluate the Radon transform at a value $v_q = 100\,\text{km s}^{-1}$. In all cases, there is a clear anisotropy and the three scenarios are easily distinguishable. This highlights the discriminatory power of directional detection. It has previously been demonstrated that only of order 10 events would be required to distinguish a directional WIMP signal from an isotropic background. Furthermore, with of order 100 events, it should be possible to detect any deviation in peak recoil direction due to a stream [256].

Say more about DD

7.3 Directional experiments

Directional experiments are still in the prototype stage, with detectors being around 1 m^3 in size, with hopes for a scale up to ton-scale experiments in the future. A number of experiments use time projection chamber (TPC) technology to achieve directional sensitivity. These include DRIFT [257, 258], NEWAGE [259, 260], MIMAC [261, 262], DMTPC [263, 264] and D3 [265].

In order to have directional sensitivity, a detector must image the tracks produced by the recoiling nucleus in the detector. The typical range of a

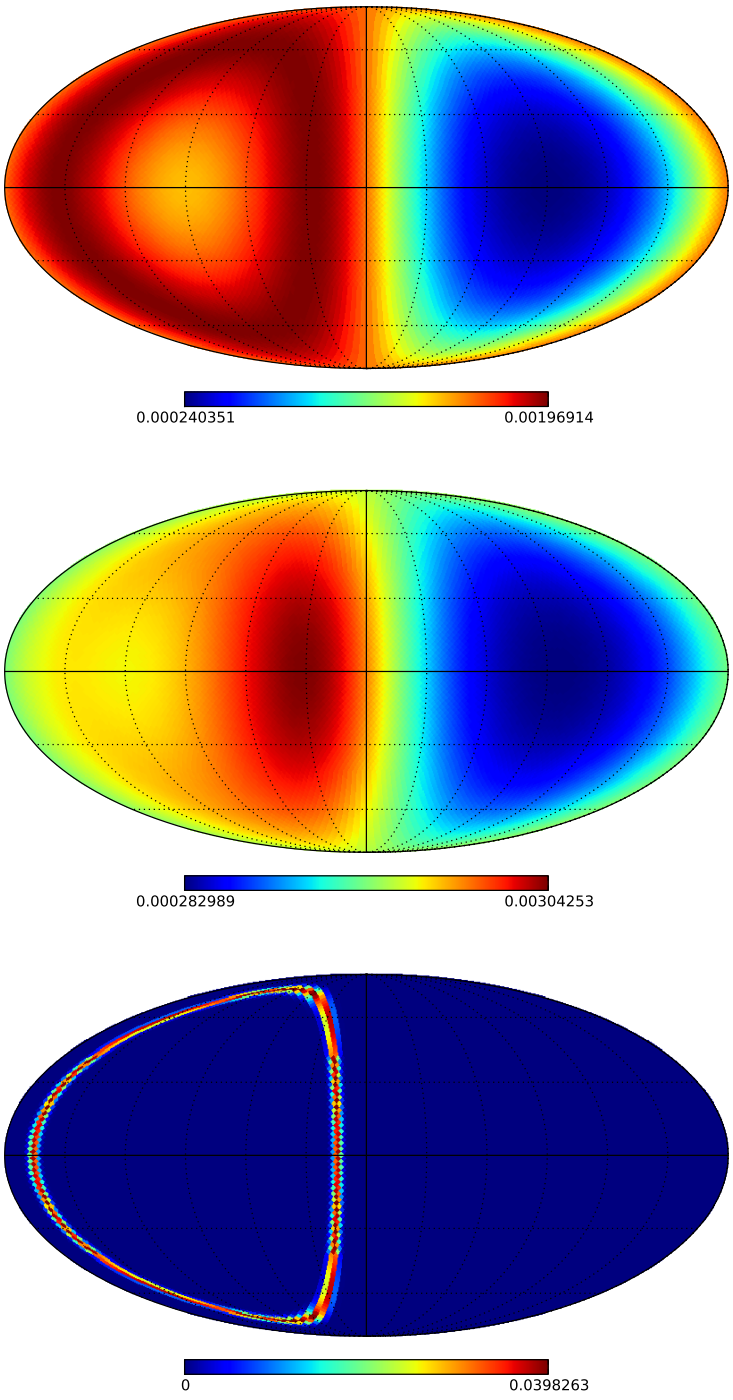

Figure 7.2: Radon transform of the SHM (top), SHM with a dark disk contribution (middle) and stream (bottom) distribution functions, evaluated at $v_q = 100\,\mathrm{km\ s^{-1}}$.

WIMP-nucleus recoil is only ∼100nm, however, which makes track reconstruction difficult. Directional experiments therefore operate in the low

pressure gas phase (around 0.05 atm [258]) in order to maximise the distance travelled by a recoiling nucleus. The detector is filled with a target gas such as CF_4 (in the case of the DRIFT experiment) which provides sensitivity to spin-dependent recoils. Nuclear recoils in the detector ionize the target gas. The freed electrons are drifted under an electric field to the faces of the detector where the charge is collected. Alternatively, an electron transport gas (CS_2 in the DRIFT experiment) may be added, which attracts the free electrons forming ions which are then collected.

The energy of the recoil can be recovered from the total amount of ionisation in the event. The three dimensional track (which is only a few mm long) can be reconstructed from the distribution of charge detected at the surface of the detector volume, with information about the z-direction obtained from the timing of the charges arriving at the surface. **Check this...** This method allows an angular resolution of 20 °-80 ° using current prototypes [266], with higher resolution at higher recoil energies. However, the sense of the recoil is much more difficult to determine, requiring sensitivity to tiny asymmetries between the start and end of the track. While sense discrimination has previously been demonstrated [267], it cannot be achieved with 100% efficiency. Even for high energy (100 keV) recoils, studies suggest that only partial sense recognition may be possible (with only a 65% probability of correctly determining the sense) [266]. Without sense discrimination the anisotropy of the WIMP signal is reduced and roughly 3 times more events are required to establish the directionality of the signal and distinguish from an anisotropic background [256, 268].

Talk about anodes rather than surfaces...

Background - Radon progeny; fiducialisation; thresholds

A number of other directional technologies have also been suggested. Nuclear emulsion experiments use as a target silver halide crystals suspended in gelatin [269]. The emulsion required must be composed of very fine grains in order to image dark matter recoil tracks smaller than 1 μm, however angular resolutions below 20 ° may be achievable. DNA based experiments [185] have also been proposed which may be able to achieve directional sensitivity. The main TPC-based experiments are in cooperation and are ultimately aiming to construct a ton-scale 'CYGNUS' detector [270].

7.4 Reconstructing the velocity distribution

With promising developments in directional detector technology, it is interesting to ask what information about the velocity distribution we could, in principle, extract from a directional signal. Alves, Hendri and Wacker [271] investigated the possibility of describing $f(\mathbf{v})$ in terms of a series of special functions of integrals of motion (energy and angular momentum). These can then be fit to data, with around 1000 events required to distinguish between the SHM and a Via Lactea II distribution function [272]. However, the special, separable form of the velocity distribution requires that the dark matter halo is in equilibrium. Moreover, this method requires an *a priori* knowledge of the DM mass (for example from earlier non-directional detectors or from collider experiments).

A more general parametrisation for the velocity distribution was recently proposed by Lee [273]. In this approach, the velocity distribution is decomposed into products of Fourier-Bessel functions and spherical harmonics. This is completely general and does not require that the halo is completely virialised. Lee also gives an analytic expression for the Radon transform of the Fourier-Bessel basis, making this approach computationally efficient. However, this basis does not guarantee that the resulting $f(\mathbf{v})$ is everywhere positive and therefore not all combinations of coefficients correspond to physical distribution functions. **Might be a good idea after a large number of events have been found...**

In fact, any decomposition in terms of spherical harmonics leads to this problem. It is unclear how this issue will affect parameter reconstruction. Without some criteria which determines which coefficients of the spherical harmonics lead to strictly positive distribution functions, it may be necessary to numerically test each parametrised distribution function for negative values. However, for a real function of three parameters $f(\mathbf{v}) = f(v_x, v_y, v_z)$ this would require a very large number of evaluations, which may not be computationally feasible. In addition, it is not clear how this property would affect an exploration of the parameter space using, for example, Markov Chain Monte Carlo or Nested Sampling [**?**]. Physical distribution functions may occupy only a small fraction of the total space of parameters or may be distributed over a large number of irregular regions in the parameter space, making sampling from them difficult.

In Sec. 7.5, I will present an alternative method of parametrising the velocity distribution, which can guarantee that the velocity distribution is everywhere positive and therefore represents a promising and general method for extracting information from directional experiments. However, first it will be instructive to discuss the invertibility of the Radon transform. That is, given a perfect realisation of the directional recoil spectrum, can we perfectly reconstruct the corresponding velocity distribution.

Point out that this is harder when you have a full 3-D function...?

7.4.1 Invertibility of the Radon transform

Make sure to check and improve the terminology - especially 'null functions'

It has been shown that for distributions $f(\mathbf{v})$ which are rapidly decreasing at infinity [274] or which are compactly supported [275], the Radon Transform is one-to-one and is therefore exactly invertible. This inversion is typically unstable (that is, the reconstructions are very sensitive to noise in the signal) and ill-posed (as not all functions are valid Radon Transforms). However, assuming that $\hat{f}$ is a valid Radon Transform and that we have full knowledge of it, we can reconstruct $f(\mathbf{v})$ exactly.

However, due to finite energy thresholds, we do not have access to the low-speed region of $\hat{f}(v_{\rm min}, \hat{q})$. We must therefore consider the related Exterior Radon Transform $\mathcal{R}_E$. Only using values of the Radon Transform for $v_{\rm min} > v_a$, is it possible to reconstruct $f(\mathbf{v})$ for $v > v_a$? If f is rapidly decreasing at infinity, this transform is still one-to-one, as in the complete case. However, if f decays as an inverse power of v (i.e. $f \sim v^{-k}$ as $v \to \infty$) the Exterior Transform is no longer one-to-one [276]. *Define null space...* In this case, the null space in 3 dimensions is non-trivial [277], consisting of functions of the form:

$$f_N(\mathbf{v}) = \frac{\alpha}{v^{3+k}} Y_{lm}(\hat{\mathbf{v}}), \tag{7.18}$$

where α is some constant, Y_{lm} is a spherical harmonic, $0 \leq k < l$ and $l - k$ is even. This means that there are no null functions for $l = 0$ or $l = 1$. It can be shown by explicit calculation that such functions have a Radon Transform of zero for all $v_{\rm min} > 0$.

In the case of direct detection, the point at $v = v_{\rm min} = 0$ corresponds to DM particles at rest with respect to the detector, which can impart no recoil energy and are therefore undetectable. For directional detection

then, even for infinitesimally small threshold energies, we must consider the Exterior Radon Transform.

This means that for a given Radon transform, adding any combination of functions of the form $f_N(\mathbf{v})$ to $f(\mathbf{v})$ leads to the same Radon transform. However, we note that the spherical harmonics with $l > 0$ can take negative values. However, at large values of v, $f_{\rm SHM}$ decays exponentially. By contrast, f_N decays as a power of v, meaning at some (potentially large) value of v the magnitude of the null function will exceed that of $f(\mathbf{v})$ leading to a negative distribution function. A more general distribution function will have a natural cut-off (say at the galactic escape speed) and will certainly decay rapidly to zero for high values of v. As a result, we can neglect the impact of null functions on reconstructions.

Thus, as long as we choose basis functions which are everywhere positive and therefore physically valid, we ensure that the Radon transform is invertible. This means that no information is lost in reconstructing $f(\mathbf{v})$ and also that there are no unphysical degeneracies present in the parametrisation we have chosen.

NB: Make it very clear that if we choose a parametrisation which can be somewhere negative (even if it's a high energies where these things don't matter because its above threshold and only a small effect), it can lead to problems of non-invertibility and introduce unphysical degeneracies in the parametrisation. Therefore it is very important to make sure that $f(\boldsymbol{v})$ is everywhere positive. I should include some plots of the null functions and of truncated null functions (added to $f(\boldsymbol{v})$) to indicate what can go wrong - and how bad things can be. Also, talk about truncated null functions and check that if we ensure positive-definiteness then truncated null functions shouldn't cause a problem... Double-check to see if truncated null functions (truncated at the same place as the full distribution function) are still null (they shouldn't be, don't just look along one direction, but all... IT DEFINITELY IS NOT NULL, SO THAT'S FINE...)

Also say that I don't think that this has previously been discussed...

7.5 Discretising the velocity distribution

In order to ensure that the velocity distribution is everywhere positive, we propose an alternative methodology. We propose that the velocity dis-

tribution be discretised into N angular components, each described by a single function of the WIMP speed:

$$f(\mathbf{v}) = f(v, \cos\theta', \phi') = \begin{cases} f_1(v) & \text{for } \theta' \in [0, \pi/N] \ , \\ f_2(v) & \text{for } \theta' \in [\pi/N, 2\pi/N] \ , \\ \vdots & \\ f_k(v) & \text{for } \theta' \in [(k-1)\pi/N, k\pi/N] \ , \\ \vdots & \\ f_N(v) & \text{for } \theta' \in [(N-1)\pi/N, \pi] \ . \end{cases} \tag{7.19}$$

We consider for simplicity only a discretisation in $\cos\theta'$, though this can be extended to an additional discretisation in ϕ' if required.

The motivation for this description is that the simplest signal (beyond an isotropic $N = 1$ signal) which can be observed with a directional detectors is a discrete asymmetry (between the event rates in, say, the forward and backward directions). Shortly after the confirmation of a dark matter signal at a directional detector, the number of events may still be quite small (for example, the roughly 10 events required to distinguish from an isotropic background). In this small statistics scenario, constraining a large number of free functions is not feasible. However, if we discretise $f(\mathbf{v})$ into $N = 2$ angular components, it should be possible to extract some meaningful directional information with only a small number of events. With larger numbers of events, N can be increased to allow more directional information to be extracted. **Improve justification...**

Because angular information is being lost from the velocity distribution, we cannot consider using the full Radon transform to constrain the functions $f_k(v)$, as this contains additional angular information. Instead, we should consider integrated Radon transforms of the form:

$$\hat{f}_k(v_{\min}) = \int_{\phi=0}^{2\pi} \int_{(k-1)\pi/N}^{k\pi/N} \hat{f}(v_{\min}, \hat{\mathbf{q}}) \, \mathrm{d}\cos\theta \mathrm{d}\phi, \tag{7.20}$$

where $\hat{\mathbf{q}} = (\cos\theta, \phi)$. Thus, we will be using a discretised version of the Radon transform (or equivalently, the event rate and, ultimately, data) in order to constrain the functional form of a discretised velocity distribution. **Improve this justification and/or swap this paragraph with the one before it...**

What form should be used for the free functions $f_k(v)$? This discretisation scheme does not depend on choosing a particular form for the v dependence of the velocity distribution. We can therefore choose any parametrisation for $f_k(v)$ - such as those described in Sec. **??** - having convinced ourselves that they introduce no bias into the fitting procedure. The question we will address here is what *angular* errors are introduced by such a discretisation. We will now demonstrate for the cases of $N = 1, 2, 3$ how the corresponding Radon transform is calculated and how it compares to the true Radon transform for some benchmark cases.

Talk somewhere about tomography...

7.5.1 $N = 1$ discretisation

The $N = 1$ case corresponds to the assumption that $f(\mathbf{v})$ is isotropic. That is, we could consider setting $f(\mathbf{v})$ equal to its angular average: $f(\mathbf{v}) = \bar{f}(v) \equiv \frac{1}{4\pi} \int f(\mathbf{v})\, \mathbf{d}\Omega_v$. The Radon transform then reduces to

$$\hat{f}\left(v_{\rm min}, \hat{\mathbf{q}}\right) = \int \delta\left(v_{\rm min} - \mathbf{v}\cdot\hat{\mathbf{q}}\right) \bar{f}(v)\, \mathrm{d}^3\mathbf{v}\,. \tag{7.21}$$

We can rewrite the delta function as

$$\delta\left(v_{\rm min} - \mathbf{v}\cdot\hat{\mathbf{q}}\right) = \frac{1}{v}\delta(v_{\rm min}/v - \hat{\mathbf{v}}\cdot\hat{\mathbf{q}})\,, \tag{7.22}$$

which means that Eq. 7.21 becomes

$$\hat{f}\left(v_{\rm min}, \hat{\mathbf{q}}\right) = \int_{v=0}^{\infty} \frac{v^2 \bar{f}(v)}{v} \oint \delta\left(v_{\rm min}/v - \hat{\mathbf{v}}\cdot\hat{\mathbf{q}}\right)\, \mathrm{d}\Omega_v \mathrm{d}v\,. \tag{7.23}$$

The angular integral evaluates to unity as long as $v_{\rm min}/v = \hat{\mathbf{v}}\cdot\hat{\mathbf{q}}$ for some value of $\hat{\mathbf{v}}$ in the domain of integration. Because we integrate over all directions $\hat{\mathbf{v}}$, this is guaranteed to be satisfied for some value, as long as $v > v_{\rm min}$ (because $\hat{\mathbf{v}}\cdot\hat{\mathbf{q}}$ cannot exceed unity). Thus,

$$\oint \delta\left(v_{\rm min}/v - \hat{\mathbf{v}}\cdot\hat{\mathbf{q}}\right)\, \mathrm{d}\Omega_v = \Theta(v - v_{\rm min})\,, \tag{7.24}$$

and

$$\hat{f}\left(v_{\rm min}, \hat{\mathbf{q}}\right) = \int_{v=v_{\rm min}}^{\infty} \frac{v^2 \bar{f}(v)}{v} \mathrm{d}v\,. \tag{7.25}$$

Finally, to obtain the directionally averaged Radon transform $\hat{f}(v_{\rm min})$, we integrate over all directions $\hat{\mathbf{q}}$. As the Radon transform is isotropic in

this case, this gives a contribution of 4π. Replacing the expression for $\bar{f}(v)$ with the directionally averaged velocity distribution, we therefore obtain **What should I call the directionally averaged RT?**

$$\hat{f}\left(v_{\min}\right) = \int_{v=v_{\min}}^{\infty} \frac{f(\mathbf{v})}{v} \mathrm{d}^3\mathbf{v}\,. \tag{7.26}$$

This matches the expression for the total non-directional scattering rate. While we assumed here that $f(v)$ was isotropic, in first deriving this expression in Chapter **??**, no such assumption was required **Was it?**. We therefore see that in the $N = 1$ case, the angular-discretised 'approximation' is in fact exact and leads to the correct angular-averaged Radon transform.

7.5.2 $N = 2$ discretisation

For the $N = 2$ case, we are considering a forward-backward asymmetry in the velocity distribution:

$$f(\mathbf{v}) = \begin{cases} f_1(v) & \text{if } \theta' \in [0, \pi/2] \\ f_2(v) & \text{if } \theta' \in [\pi/2, \pi]\,. \end{cases} \tag{7.27}$$

From these, we wish to obtain the integrated recoil spectra for the forward and back directions. Specifically:

$$\hat{f}_1 = \int_0^1 \hat{f}(v_q, \cos\theta)\, \mathrm{d}\cos\theta \tag{7.28}$$

$$\hat{f}_2 = \int_{-1}^0 \hat{f}(v_q, \cos\theta)\, \mathrm{d}\cos\theta\,. \tag{7.29}$$

We will focus on the first of these, $\hat{f}_1$, as the other can be obtained simply by exchanging which directions are forward and backward (that is, by interchanging f_1 and f_2). From now on, we will therefore be working under the assumption that $\cos\theta \in [0, 1]$.

We first consider calculating the azimuthally averaged Radon transform:

$$\hat{f}(v_q, \cos\theta) = \int_0^{2\pi} \hat{f}(v_q, \cos\theta, \phi)\, \mathrm{d}\phi \tag{7.30}$$

$$= \int_0^{2\pi} \left(\int_{\mathbb{R}^3} f(\mathbf{v}) \delta\left(\mathbf{v}\cdot\hat{\mathbf{q}} - v_q\right)\, \mathrm{d}^3\mathbf{v} \right) \mathrm{d}\phi \tag{7.31}$$

$$= \int_{\phi=0}^{2\pi} \int_{v=0}^{\infty} \oint v f(\mathbf{v}) \delta\left(v_{\rm min}/v - \hat{\mathbf{v}}\cdot\hat{\mathbf{q}}\right)\, \mathrm{d}\Omega_v \mathrm{d}v \mathrm{d}\phi\,. \tag{7.32}$$

We focus on performing the ϕ integral, which we define as:

$$I(v_q, \cos\theta, \mathbf{v}) = \int_0^{2\pi} \delta\left(\sin\theta\sin\theta'\cos(\phi-\phi') + \cos\theta\cos\theta' - v_q/v\right)\, \mathrm{d}\phi \tag{7.33}$$

$$\equiv \int_0^{2\pi} \delta\left(g(\phi)\right)\, \mathrm{d}\phi\,. \tag{7.34}$$

We then rewrite the delta function as a function of ϕ:

$$\delta\left(g(\phi)\right) = \sum_i \frac{\delta(\phi-\phi_i)}{|g'(\phi_i)|}\,. \tag{7.35}$$

Here, we sum over those values of ϕ_i satisfying $g(\phi_i) = 0$. We leave the details of the full calculation to Appendix **??**. However, we obtain,

$$I(v_q, \cos\theta, \mathbf{v}) = \frac{2C(\alpha)}{\sqrt{(\sin\theta\sin\theta')^2 - (\beta - \cos\theta\cos\theta')^2}} \Theta(v - v_q)\,, \tag{7.36}$$

where

$$\beta = v_q/v\,; \qquad \alpha = \frac{\beta - \cos\theta\cos\theta'}{\sin\theta\sin\theta'}\,, \tag{7.37}$$

and $C(\alpha) = 1$ for $\alpha \in [-1, 1]$ and vanishing otherwise.

We therefore obtain

$$\hat{f}(v_q, \cos\theta) = \int_{v=v_q}^{\infty} \int_{\cos\theta=-1}^{1} \int_{\cos\theta'=-1}^{1} f(v, \cos\theta') I(v_q, \cos\theta, v, \cos\theta')\, v\mathrm{d}v\mathrm{d}\cos\theta\mathrm{d}\cos\theta'\,, \tag{7.38}$$

with

$$f(v, \cos\theta') = \int_0^{2\pi} f(v, \cos\theta', \phi')\, \mathrm{d}\phi'\,. \tag{7.39}$$

Leave a load of the details for the appendix

In the $N = 2$ case, we obtain

$$\hat{f}_1 = 4\pi \int_{v_q}^{\infty} v \left(\pi f_1(v) + \tan^{-1} \left\{ \frac{\sqrt{1-\beta^2}}{\beta} \right\} (f_2(v) - f_1(v)) \right) \mathrm{d}v \quad (7.40)$$

$$\hat{f}_2 = 4\pi \int_{v_q}^{\infty} v \left(\pi f_2(v) + \tan^{-1} \left\{ \frac{\sqrt{1-\beta^2}}{\beta} \right\} (f_1(v) - f_2(v)) \right) \mathrm{d}v \,. \quad (7.41)$$

We have also checked using Monte Carlo calculations that these are the correct forms of the forward and backward averaged Radon transforms in the case of a discretised velocity distribution.

We now wish to compare these approximate Radon transforms with the Radon transforms obtained from the full (non-discretised) velocity distribution. To do this, we select a benchmark velocity distribution (such as the SHM) and calculate $f_{1,2}$ according to Eq. 7.27 by averaging over the $\cos\theta'$ in the forward and backward directions. This discretised velocity distribution is shown in Fig. 7.5.2. We then insert these into Eq. 7.40 to obtain the forward and backward Radon transform. For comparison, we use the full velocity distribution of Eq. 7.15 to obtain the *true* forward and backward Radon transforms by integrating over $\cos\theta$.

The results of this comparison for a SHM model with $v_{\rm lag} = 220\,\mathrm{km\ s^{-1}}$ and $\sigma_v = 156\,\mathrm{km\ s^{-1}}$ are shown in Fig. 7.5.2. While the general features are reproduced, there are some discrepancies. In particular, the forward Radon transform obtained using the approximate method is roughly 80% of the correct result, while the backward Radon transform is up to 100% larger using the approximate method. The reason for this is clear from Fig. 7.5.2, which shows that the discretised velocity distribution has a greater fraction of WIMPs with velocities at right angles to the forward direction ($\theta' = 0$). Thus, the discretised velocity distribution has a greater chance of producing scatters in the backward direction. Overall, the discretised distribution is less focused in the forward direction, resulting in a reduced asymmetry between the forward and backward scattering rates.

These discrepancies between the true and approximate recoil spectra may prove problematic when this method is employed in parameter estimation and the reconstruction of $f(\mathbf{v})$. However, these discrepancies should be redued when the finite angular resolution of detectors is taken into account. *Mention finite angular resolution...Do some plots...*

Consider a more radical distribution - such as a stream and show that it doesn't work so well...

7.5.3 $N = 3$ discretisation

Given the discrepancies in the $N = 2$ case, we will now consider the $N = 3$ discretisation, which should improve the fit between the true and approximate distribution. In addition, the $N = 3$ will allow us to employ this methodology to the case where sense discrimination of recoils is not possible. Without sense discrimination, the forward and backward directions cannot be distinguished and the $N = 2$ discretisation provides no directional sensitivity. As we shall see shortly, directional sensitivity is possible in the $N = 3$ case.

We write the velocity distribution in discretised form as

$$f(\mathbf{v}) = \begin{cases} f_1(v) & \text{if } \theta' \in [0, \pi/3] \\ f_2(v) & \text{if } \theta' \in [\pi/3, 2\pi/3] \\ f_3(v) & \text{if } \theta' \in [2\pi/3, \pi]\,. \end{cases} \tag{7.42}$$

If we interpret this discretisation as an averaging of the underlying velocity distribution, as before, we obtain the distribution in the bottom panel of Fig. 7.5.3 (the full SHM distribution is shown in the top panel for reference). Following the same procedure as for the $N = 2$ case, we can obtain the corresponding forward, backward and transverse Radon transforms. The exact form of these is complicated (and not particularly instructive). However, this form can be generated using the algorithm described in Sec. **??**, in which we treat the case of general N.

Again, we wish to test how closely the $N = 3$ discretised distribution can reproduce the true forward-, backward- and transverse-averaged Radon transforms. The results are shown in Fig. 7.5.2. Compared to the $N = 2$ case, the recoil spectra are reproduced much more closely, with a discrepancy of at most 15% **check** between the true and approximate distributions.

Emphasise that we haven't included the form factors...

The folded distribution

As discussed in Sec. 7.3, sense discrimination between forward and backward-going recoils may not be possible with near-future detectors. In this case

then, all that can be measured is the so called 'folded' recoil spectrum

$$\frac{\mathrm{d}R}{\mathrm{d}E_R \mathrm{d}|\cos\theta|} = \frac{\mathrm{d}R}{\mathrm{d}E_R \mathrm{d}\cos\theta} + \frac{\mathrm{d}R}{\mathrm{d}E_R \mathrm{d}(-\cos\theta)} \,. \tag{7.43}$$

As a result, we are concerned not will the full Radon transform of $f(\mathbf{v})$, but the folded Radon transform $\hat{f}(v_q, |\cos\theta|)$. In the case of $N = 2$ discretisation, this folded Radon transform would have no directional information (because the forward and backward scattering rates differ only in the sign of $\cos\theta$). However, in the $N = 3$ case, the transverse Radon transform, given by **define this earlier in the text...**

$$\hat{f}_T(v_q) = \hat{f}_2(v_q) = \int_{-1/2}^{1/2} \hat{f}(v_q, \cos\theta)\, \mathrm{d}\cos\theta \,, \tag{7.44}$$

is invariant under $\hat{f}(v_q, \cos\theta) \to \hat{f}(v_q, |\cos\theta|)$ (apart from an overall factor of 2). That is, the transverse event rate 'folds' back onto itself. Thus, even without sense discrimination, directional experiments will still be sensitive to this transverse scattering rate. By comparison, if the forward and backward directions cannot be distinguished, the remaining two averaged Radon transforms (the top two panels in Fig. 7.5.3) are folded together, to obtain the longitudinal rate

$$\hat{f}_L(v_q) = \int_{-1}^{-1/2} \hat{f}(v_q, \cos\theta)\, \mathrm{d}\cos\theta + \int_{1/2}^{1} \hat{f}(v_q, \cos\theta)\, \mathrm{d}\cos\theta \,. \tag{7.45}$$

We plot the transverse and longitudinal averaged in Fig. 7.5.3. **Need a factor of 2 in the transverse bit...?** As expected, the two rates are now more similar in shape as we have lost some directional information. The approximate Radon transforms, obtained from the discretisation, match the true transforms closely for speeds above $v_q \approx 200\,\mathrm{km\ s^{-1}}$. **Why the discrepancy at low v?** For realistic experiments, these low speeds will be below the threshold energy of the experiment and the bias introduced by this discrepancy should be minimal **find some numbers for this...**.

We note that in this folded case, we would fit to two functions, corresponding to the longitudinal and transverse event rates. However, our original discretisation required 3 free functions of v: $f_{1,2,3}(v)$. However, due to the properties of the Radon transform **(which are...?)**, the longitudinal rate is not a function of $f_1(v)$ and $f_3(v)$ but of the sum $f_1(v)+f_3(v) \equiv f_L(v)$. Thus, we have only two free functions to fit $f_{L,T}(v)$.

-Fix captions on figures...

-Discuss a dark disk case...

-Discuss the poorly aligned - off axis case...

7.6 Discretisation for general N

The procedure which has been described above can be extended to any number N of angular bins. Significantly, for any value of N, the resulting Radon transform remains a sum of elementary, analytic functions multiplied by one dimensional functions $f_k(v)$. This means that no angular integration must be performed in order to obtain the Radon transform and at most N one-dimensional integrals over the velocity v must be performed, one for each of the $\hat{f}_k(v_q)$.

While the details of the calculation can be found in Appendix **??**, we show below the full algorithm for calculating the averaged Radon transforms from a velocity distribution discretised into N angular pieces...

FINISH

7.7 Conclusion

Check consistency with vmin and vq..., be careful about f's with subscript 1
Check notation consistency with lefts(and rights) **We can even combine this with the non-directional experiments...**

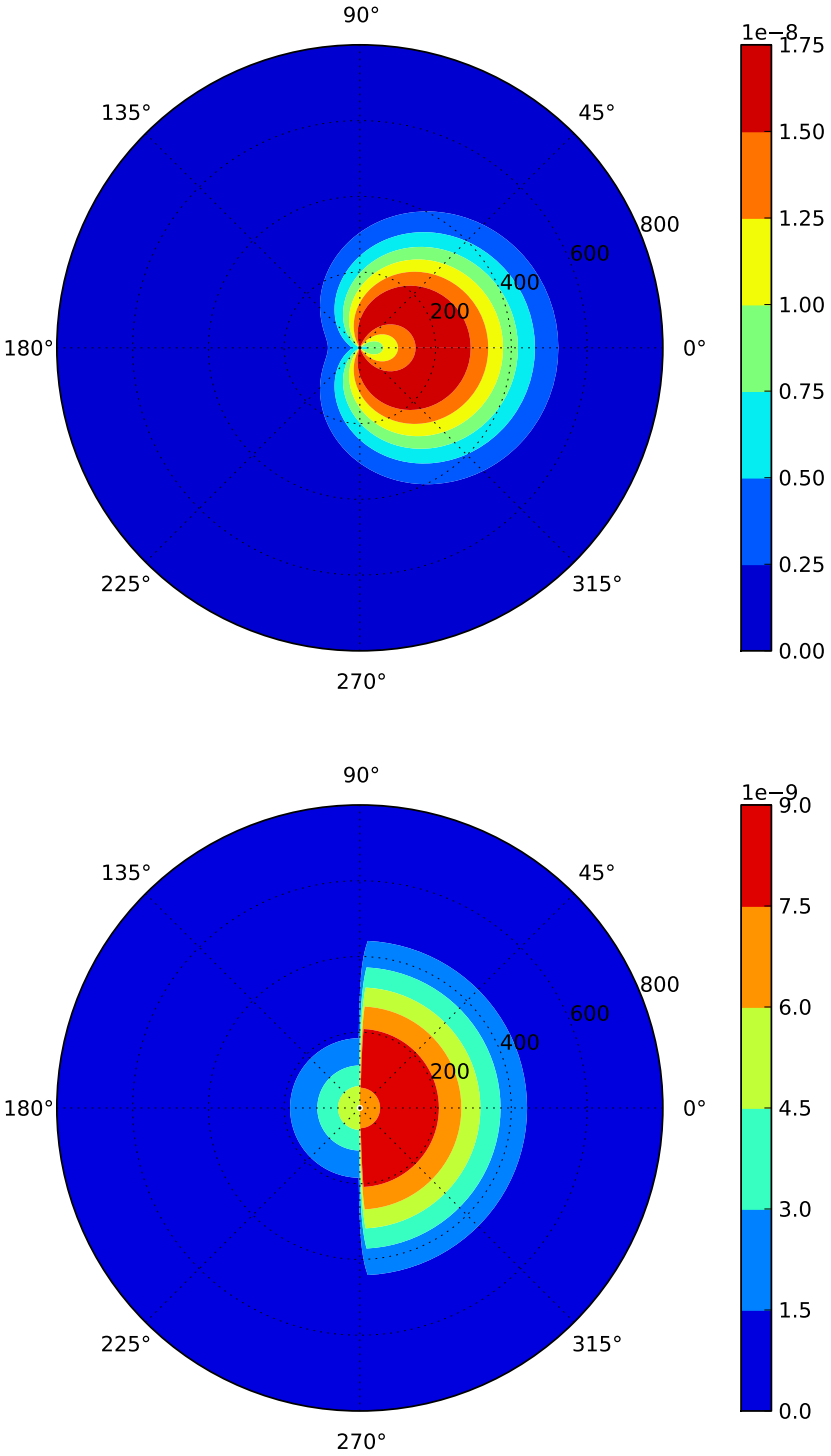

Figure 7.3: Polar plots in (v, θ') for two velocity distributions. Shown are the SHM velocity distribution for $v_{\rm lag} = 220\,{\rm km\ s^{-1}}$ and $\sigma_v = 156\,{\rm km\ s^{-1}}$ (top) and the discretised SHM distribution obtained by averaging in the forward and backward directions (bottom). The vector $\mathbf{v}_{\rm lag}$ is aligned along $\theta' = 0$. Note the different color scales in the two plots.

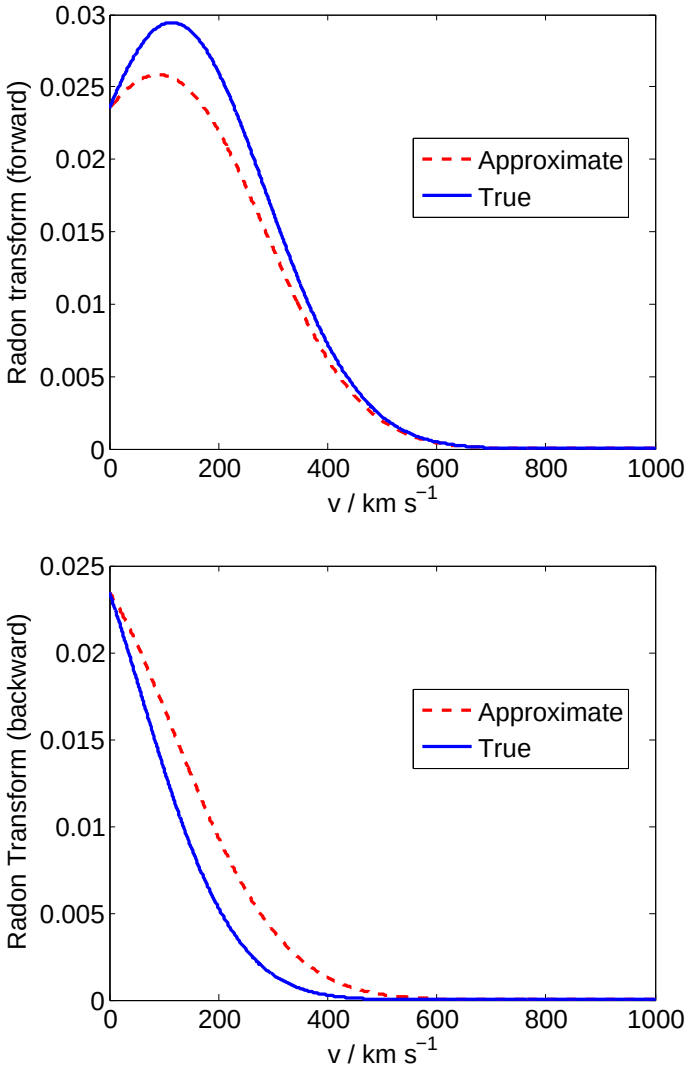

Figure 7.4: True and approximate forward and backward radon transforms when the full velocity distribution is discretised into N = 2 directional pieces. **Finish**

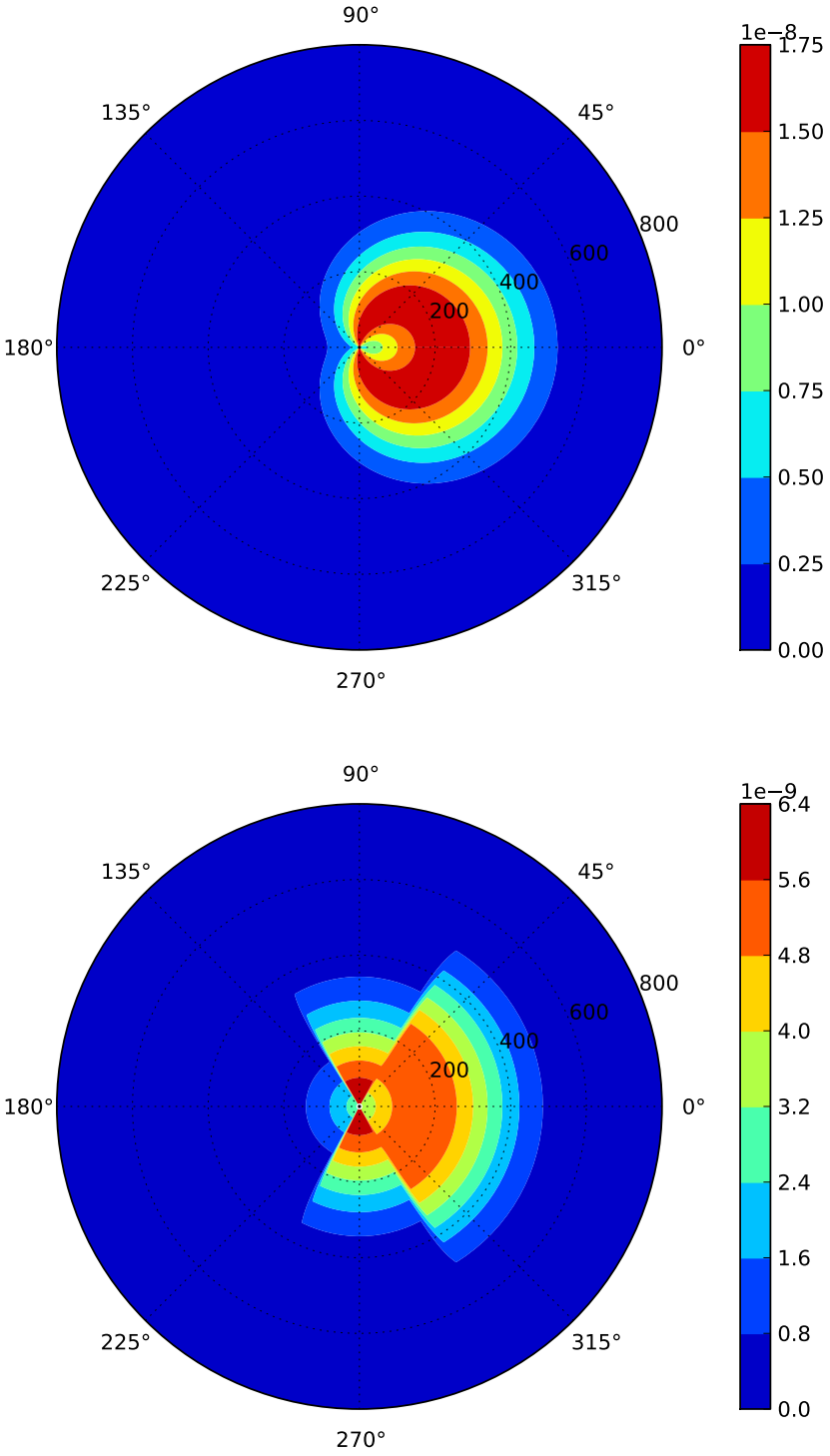

Figure 7.5: Polar plots in (v, θ') for two velocity distributions. Shown are the SHM velocity distribution for $v_{\rm lag} = 220\,{\rm km\ s^{-1}}$ and $\sigma_v = 156\,{\rm km\ s^{-1}}$ (top) and the discretised SHM distribution obtained by averaging in the forward, backward and transverse directions (bottom). The vector $\mathbf{v}_{\rm lag}$ is aligned along $\theta' = 0$. Note the different color scales in the two plots.

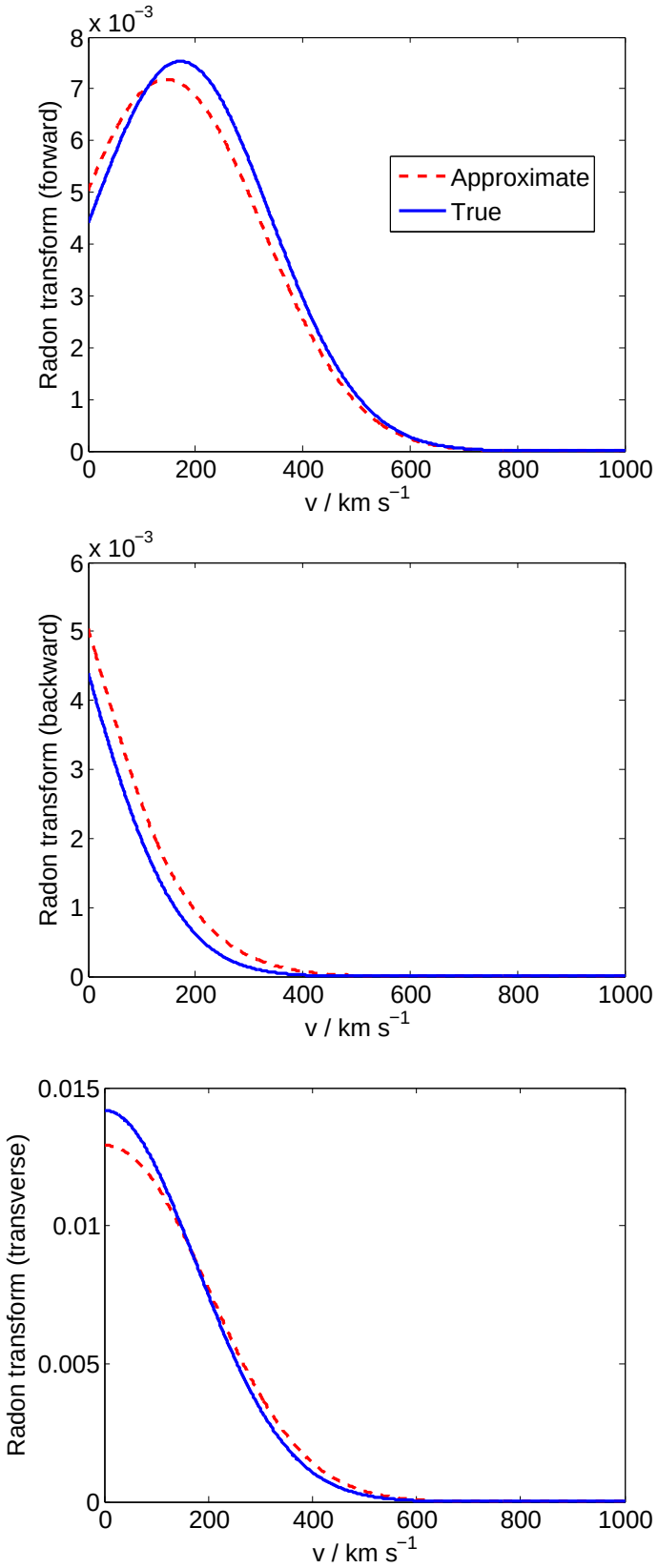

Figure 7.6: True and approximate transforms when the full velocity distribution is discretised into N = 3 directional pieces. In the 'forward' case $\cos\theta \in [1/2, 1]$, in the 'backward' case $\cos\theta \in [-1, -1/2]$, and in the 'transverse case' $\cos\theta \in [-1/2, 1/2]$.

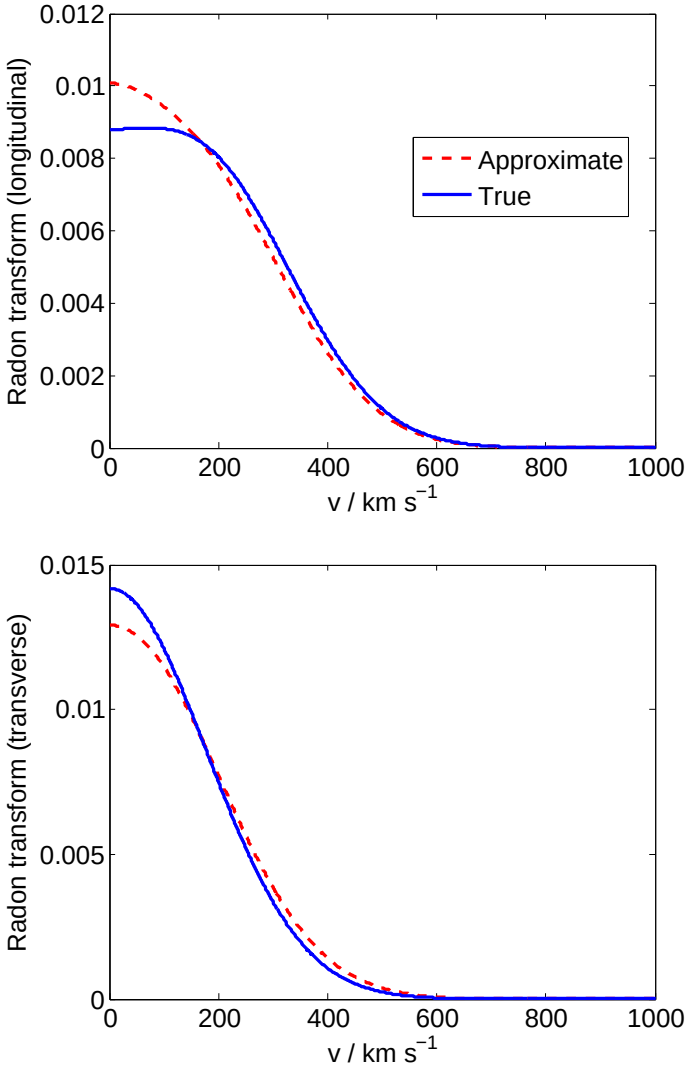

Figure 7.7: True and approximate folded transforms when the full velocity distribution is discretised into N = 3 directional pieces. In the 'longitudinal' case $|\cos\theta| \in [1/2, 1]$ while in the 'transverse case' $|\cos\theta| \in [0, 1/2]$.

Chapter 8

Conclusions

Bibliography

[1] A. G. Riess, *et al.*, Astrophys. J. **116**, 1009 (1998), astro-ph/9805201 .

[2] S. Perlmutter, *et al.*, Astrophys. J. **517**, 565 (1999), astro-ph/9812133 .

[3] E. W. Kolb and M. S. Turner, *The Early Universe* (Addison-Wesley, Reading, Massachusetts, 1990) Chap. 9.

[4] G. Hinshaw, *et al.*, Astrophys. J. Suppl. Ser. **208**, 19+ (2013).

[5] C. J. MacTavish, *et al.*, Astrophys. J. **647**, 799 (2005), astro-ph/0507503 .

[6] K. S. Dawson, *et al.*, Astron. J. **145**, 10+ (2013).

[7] P. A. R. Ade, *et al.* (BICEP2 Collaboration), (2014), arXiv:1403.3985 .

[8] T. D. Kitching, *et al.*, (2014), arXiv:1401.6842 .

[9] P. A. R. Ade *et al.* (Planck Collaboration), (2013), arXiv:1303.5062 .

[10] P. A. R. Ade *et al.* (Planck Collaboration), Astron. Astrophys. (2014), arXiv:1303.5076 .

[11] F. Zwicky, Helv. Phys. Acta. **6**, 110 (1933).

[12] J. S. Sanders, A. C. Fabian, E. Churazov, A. A. Schekochihin, A. Simionescu, S. A. Walker, and N. Werner, Science **341**, 1365 (2013), arXiv:1309.4866 .

[13] R. Fusco-Femiano and J. P. Hughes, Astrophys. J. **429**, 545+ (1994).

[14] N. Makino, Publ. Astron. Soc. Jpn. **46**, 139 (1994).

[15] N. Okabe, G. P. Smith, K. Umetsu, M. Takada, and T. Futamase, Astrophys. J. **769**, L35 (2013), arXiv:1302.2728 .

[16] S. Ettori, A. Donnarumma, E. Pointecouteau, T. H. Reiprich, S. Giodini, L. Lovisari, and R. W. Schmidt, Space Sci. Rev. **177**, 119 (2013), arXiv:1303.3530 .

[17] R. G. Carlberg, H. K. C. Yee, E. Ellingson, R. Abraham, P. Gravel, S. Morris, and C. J. Pritchet, Astrophys. J. **462**, 32+ (1996), arXiv:astro-ph/9509034 .

[18] V. Springel, *et al.*, Nature **435**, 629 (2005), arXiv:astro-ph/0504097 .

[19] J. Diemand, M. Kuhlen, and P. Madau, Astrophys. J. **657**, 262 (2006), astro-ph/0611370 .

[20] V. Springel, J. Wang, M. Vogelsberger, A. Ludlow, A. Jenkins, A. Helmi, J. F. Navarro, C. S. Frenk, and S. D. M. White, Mon. Not. R. Astron. Soc. **391**, 1685 (2008), arXiv:0809.0898 .

[21] G. Stinson, J. Bailin, H. Couchman, J. Wadsley, S. Shen, C. Brook, and T. Quinn, Mon. Not. R. Astron. Soc. **408**, 812 (2010), arXiv:1004.0675 .

[22] M. L. Norman and G. L. Bryan, "Cosmological adaptive mesh refinement," in *Numerical Astrophysics 1998*, Vol. 240, edited by S. M. Miyama, K. Tomisaka, and T. Hanawa (Springer Netherlands, Dordrecht, 1999) Chap. 3, pp. 19–28, arXiv:astro-ph/9807121 .

[23] V. Springel, Mon. Not. R. Astron. Soc. **401**, 791 (2010), arXiv:0901.4107 .

[24] A. Pillepich, M. Kuhlen, J. Guedes, and P. Madau, Astrophys. J. **784**, 161+ (2014), arXiv:1308.1703 .

[25] M. Vogelsberger, S. Genel, D. Sijacki, P. Torrey, V. Springel, and L. Hernquist, Mon. Not. R. Astron. Soc. **436**, 3031 (2013), arXiv:1305.2913 .

[26] D. Martizzi, R. Teyssier, B. Moore, and T. Wentz, Mon. Not. R. Astron. Soc. **422** (2012), arXiv:1112.2752 .

[27] K. Begeman, A. Broeils, and R. Sanders, Mon. Not. R. Astron. Soc. **249**, 523 (1991).

[28] M. Persic, P. Salucci, and F. Stel, Mon. Not. R. Astron. Soc. **281**, 27 (1996), astro-ph/9506004 .

[29] G. Kauffmann, S. D. White, and B. Guiderdoni, Mon. Not. R. Astron. Soc. **264**, 201 (1993).

[30] M. G. Walker, M. Mateo, E. W. Olszewski, J. Peñarrubia, N. W. Evans, and G. Gilmore, Astrophys. J. **704**, 1274+ (2009).

[31] V. Belokurov, *et al.*, Astrophys. J. Lett. **712**, L103 (2010), arXiv:1002.0504 .

[32] A. Klypin, A. V. Kravtsov, O. Valenzuela, and F. Prada, Astrophys. J. **522**, 82 (1999).

[33] M. Boylan-Kolchin, J. S. Bullock, and M. Kaplinghat, Mon. Not. R. Astron. Soc. Lett. **415**, L40 (2011), arXiv:1103.0007 .

[34] S. Garrison-Kimmel, M. Boylan-Kolchin, J. S. Bullock, and E. N. Kirby, (2014), arXiv:1404.5313 .

[35] W. J. G. de Blok, Adv. Astron. **2010**, 1 (2010), arXiv:0910.3538 .

[36] J. Dubinski and R. G. Carlberg, Astrophys. J. **378**, 496+ (1991).

[37] J. F. Navarro, C. S. Frenk, and S. D. M. White, Astrophys. J. **462**, 563+ (1996), arXiv:astro-ph/9508025 .

[38] P. Salucci, Mon. Not. R. Astron. Soc. **320**, L1 (2001).

[39] F. Donato, G. Gentile, and P. Salucci, Mon. Not. R. Astron. Soc. **353**, L17 (2004), arXiv:astro-ph/0403206 .

[40] E. Hayashi, J. F. Navarro, C. Power, A. Jenkins, C. S. Frenk, S. D. M. White, V. Springel, J. Stadel, and T. R. Quinn, Mon. Not. R. Astron. Soc. **355**, 794 (2004), arXiv:astro-ph/0310576 .

[41] M. Gritschneder and D. N. C. Lin, Astrophys. J. **765**, 38+ (2013).

[42] N. C. Amorisco, J. Zavala, and T. J. L. de Boer, Astrophys. J. **782**, L39+ (2014), arXiv:1309.5958 .

[43] A. Del Popolo, J. A. S. Lima, J. C. Fabris, and D. C. Rodrigues, "A unified solution to the small scale problems of the λcdm model," (2014), arXiv:1404.3674 .

[44] B. Moore, T. Quinn, F. Governato, J. Stadel, and G. Lake, Mon. Not. R. Astron. Soc. **310**, 1147 (1999), astro-ph/9903164 .

[45] P. Bode, J. P. Ostriker, and N. Turok, Astrophys. J. **556**, 93 (2001), astro-ph/0010389 .

[46] A. V. Macciò and F. Fontanot, Mon. Not. R. Astron. Soc. Lett. **404**, L16 (2010).

[47] M. Taoso, G. Bertone, and A. Masiero, J. Cosmol. Astropart. Phys. **03**, 022 (2008), arXiv:0711.4996 .

[48] V. K. Narayanan, D. N. Spergel, R. Davé, and C.-P. Ma, The Astrophysical Journal **543**, L103 (2000), astro-ph/0005095 .

[49] J. R. Bond and A. S. Szalay, Astrophys. J. **274**, 443 (1983).

[50] D. Boyanovsky, H. J. de Vega, and N. Sanchez, Phys. Rev. D **78** (2008), arXiv:0807.0622 .

[51] K. Abazajian, E. R. Switzer, S. Dodelson, K. Heitmann, and S. Habib, Phys. Rev. D **71**, 043507 (2005), astro-ph/0411552 .

[52] R. de Putter, *et al.*, Astrophys. J. **761**, 12+ (2012), arXiv:1201.1909 .

[53] A. De Rújula, S. L. Glashow, and U. Sarid, Nucl. Phys. B **333**, 173 (1990).

[54] A. Kudo and M. Yamaguchi, Phys. Lett. B **516**, 151 (2001).

[55] T. Hemmick, *et al.*, Phys. Rev. D **41**, 2074 (1990).

[56] M. L. Perl, P. C. Kim, V. Halyo, E. R. Lee, I. T. Lee, D. Loomba, and K. S. Lackner, Int. J. Mod. Phys. A **16**, 2137 (2001), hep-ex/0102033 .

[57] S. N. Gninenko, N. V. Krasnikov, and A. Rubbia, Phys. Rev. D **75**, 075014 (2007), hep-ph/0612203 .

[58] A. Melchiorri, A. Polosa, and A. Strumia, Phys. Lett. B **650**, 416 (2007), hep-ph/0703144 .

[59] P. Natarajan, A. Loeb, J.-P. Kneib, and I. Smail, Astrophys. J. **580**, L17 (2002), astro-ph/0207045 .

[60] X. Chen, S. Hannestad, and R. J. Scherrer, Phys. Rev. D **65**, 123515 (2002), astro-ph/0202496 .

[61] A. Erickcek, P. Steinhardt, D. McCammon, and P. McGuire, Phys. Rev. D **76**, 042007 (2007), arXiv:0704.0794 .

[62] I. F. M. Albuquerque and L. Baudis, Phys. Rev. Lett. **90** (2004), astro-ph/0301188 .

[63] D. Feldman, Z. Liu, P. Nath, and G. Peim, Phys. Rev. D **81**, 095017 (2010), arXiv:1004.0649 .

[64] G. Gelmini and P. Gondolo, "DM production mechanisms," in *Particle Dark Matter*, edited by G. Bertone (Cambridge University Press, Cambridge, 2010) Chap. 7, pp. 121–141, arXiv:1009.3690 .

[65] K. Griest, Phys. Rev. D **43**, 3191 (1991).

[66] L. J. Hall, K. Jedamzik, J. March-Russell, and S. M. West, J. High Energy Phys. **2010** (2010), arXiv:0911.1120 .

[67] D. J. H. Chung, E. W. Kolb, and A. Riotto, Phys. Rev. D **59** (1998), hep-ph/9802238 .

[68] V. A. Kuzmin and I. I. Tkachev, JETP Lett. **68**, 271 (1998), hep-ph/9802304 .

[69] T. Gherghetta, G. F. Giudice, and J. D. Wells, Nucl. Phys. B **559**, 27 (1999), hep-ph/9904378 .

[70] B. Fields and S. Sarkar, J. Phys. G. **33**, 1 (2006), astro-ph/0601514 .

[71] M. Maggiore, Phys. Rep. **331**, 283 (2000), gr-qc/9909001 .

[72] R. H. Cyburt, B. D. Fields, K. A. Olive, and E. Skillman, J. Astropart. Phys. **23**, 313 (2005), astro-ph/0408033 .

[73] K. Jedamzik, Phys. Rev. D **74** (2006), hep-ph/0604251 .

[74] G. Jungman, M. Kamionkowski, and K. Griest, Phys. Rep. **267**, 195 (1995), hep-ph/9506380 .

[75] G. L. Kane and S. P. Martin, "A supersymmetry primer," in *Perspectives on Supersymmetry II*, Vol. 21 (WORLD SCIENTIFIC, Singapore, 2011) pp. 1–153, hep-ph/9709356 .

[76] J. Ellis, J. S. Hagelin, D. V. Nanopoulos, K. Olive, and M. Srednicki, Nucl. Phys. B **238**, 453 (1984).

[77] B. Shakya, "The status of neutralino dark matter," (2013), arXiv:1312.7505 .

[78] K.-Y. Choi and O. Seto, Phys. Rev. D **88**, 035005 (2013), arXiv:1305.4322 .

[79] E. W. Kolb, D. J. H. Chung, and A. Riotto, "Wimpzillas!" in *DARK98: Proceedings of the Second International Conference on Dark Matter in Astro and Particle Physics*, edited by H. V. Klapdor-Kleingrothaus and L. Baudis (AIP, 1999) pp. 91–105, hep-ph/9810361 .

[80] M. J. Duff, "Kaluza-Klein theory in perspective," (1994), hep-th/9410046 .

[81] T. Appelquist, H.-C. Cheng, and B. A. Dobrescu, Phys. Rev. D **64**, 035002 (2001), hep-ph/0012100 .

[82] H.-C. Cheng, K. T. Matchev, and M. Schmaltz, Phys. Rev. D **66**, 036005 (2002), hep-ph/0204342 .

[83] G. Servant and T. M. P. Tait, Nucl. Phys. B **650**, 391 (2002), hep-ph/0206071 .

[84] L. Bergström, *New J. Phys.*, New Journal of Physics **11**, 105006+ (2009), arXiv:0903.4849 .

[85] C. Amsler, *et al.*, Phys. Lett. B **667**, 1 (2008).

[86] S. Dodelson and L. Widrow, Phys. Rev. Lett. **72**, 17 (1994), hep-ph/9303287 .

[87] X. Shi and G. M. Fuller, Phys. Rev. Lett. **82**, 2832 (1999), astro-ph/9810076 .

[88] T. Asaka, M. Shaposhnikov, and A. Kusenko, Phys. Lett. B **638**, 401 (2006), hep-ph/0602150 .

[89] R. D. Peccei and H. R. Quinn, Phys. Rev. Lett. **38**, 1440 (1977).

[90] G. Raffelt, "Axions in astrophysics and cosmology," (1995), hep-ph/9502358 .

[91] P. Sikivie and Q. Yang, Phys. Rev. Lett. **103** (2009), arXiv:0901.1106 .

[92] C. J. Copi, D. Huterer, D. J. Schwarz, and G. D. Starkman, Adv. in Astron. **2010**, 1 (2010), arXiv:1004.5602 .

[93] A. Arvanitaki, S. Dimopoulos, S. Dubovsky, N. Kaloper, and J. March-Russell, Phys. Rev. D **81** (2010), arXiv:0905.4720 .

[94] M. Cirelli, N. Fornengo, and A. Strumia, Nucl. Phys. B **753**, 178 (2007), arXiv:hep-ph/0512090 .

[95] L. Edelhäuser, T. Flacke, and M. Krämer, J. High Energy Phys. **2013** (2013), arXiv:1302.6076 .

[96] T. Kakuda, K. Nishiwaki, K.-y. Oda, N. Okuda, and R. Watanabe, "Phenomenological constraints on universal extra dimensions at LHC and electroweak precision test," (2013), arXiv:1304.6362 .

[97] ATLAS Collaboration, `https://atlas.web.cern.ch/Atlas/GROUPS/PHYSICS/CombinedSummaryPlots/SUSY/ATLAS_SUSY_Summary/ATLAS_SUSY_Summary.pdf` (2013).

[98] CMS Collaboration, `https://twiki.cern.ch/twiki/pub/CMSPublic/SUSYSMSSummaryPlots8TeV/barplot_blue_orange_SUSY2013.pdf` (2013).

[99] N. Zhou, D. Berge, and D. Whiteson, Phys. Rev. D **87**, 095013 (2013), arXiv:1302.3619 .

[100] P. J. Fox, R. Harnik, J. Kopp, and Y. Tsai, Phys. Rev. D **85**, 056011+ (2011), arXiv:1109.4398 .

[101] H. Baer, E.-K. Park, and X. Tata, New J. Phys. **11**, 105024+ (2009), arXiv:0903.0555 .

[102] O. Buchmueller, M. J. Dolan, and C. McCabe, J. High Energy Phys. **2014** (2014), arXiv:1308.6799 .

[103] G. Busoni, A. De Simone, E. Morgante, and A. Riotto, Phys. Lett. B **728**, 412 (2013), arXiv:1307.2253 .

[104] M. Ackermann, *et al.* (Fermi-LAT), Physical Review D **86**, 022002 (2012), arXiv:1205.2739 .

[105] M. Boezio, *et al.*, New J. Phys. **11**, 105023+ (2009).

[106] M. Aguilar, *et al.* (AMS Collaboration), Physical Review Letters **110** (2013).

[107] A. Ibarra, A. S. Lamperstorfer, and J. Silk, Phys. Rev. D **89**, 063539 (2014), arXiv:1309.2570 .

[108] J. Lavalle, Q. Yuan, D. Maurin, and X. J. Bi, Astron. Astrophys. **479**, 427 (2008), arXiv:0709.3634 .

[109] M. Ackermann, *et al.* (Fermi-LAT Collaboration), Phys. Rev. D **89**, 042001 (2014), arXiv:1310.0828 .

[110] C. Weniger, J. Cosmol. Astropart. Phys. **2012**, 007 (2012), arXiv:1204.2797 .

[111] E. Bloom, E. Charles, E. Izaguirre, A. Snyder, A. Albert, B. Winer, Z. Yang, and R. Essig, "Search of the earth limb fermi data and Non-Galactic center region fermi data for signs of narrow lines," (2013), arXiv:1303.2733 .

[112] W. Buchmüller and M. Garny, J. Cosmol. Astropart. Phys. **2012**, 035 (2012), arXiv:1206.7056 .

[113] T. Cohen, M. Lisanti, T. R. Slatyer, and J. G. Wacker, J. High Energy Phys. **2012** (2012), arXiv:1207.0800 .

[114] L. Goodenough and D. Hooper, "Possible evidence for dark matter annihilation in the inner milky way from the fermi gamma ray space telescope," (2009), arXiv:0910.2998 .

[115] D. Hooper and L. Goodenough, Phys. Lett. B **697**, 412 (2011), arXiv:1010.2752 .

[116] A. Boyarsky, D. Malyshev, and O. Ruchayskiy, Phys. Lett. B **705**, 165 (2010), arXiv:1012.5839 .

[117] K. N. Abazajian, J. Cosmol. Astropart. Phys. **2011**, 010 (2011), arXiv:1011.4275 .

[118] T. Daylan, D. P. Finkbeiner, D. Hooper, T. Linden, S. K. N. Portillo, N. L. Rodd, and T. R. Slatyer, "The characterization of the Gamma-Ray signal from the central milky way: A compelling case for annihilating dark matter," (2014), arXiv:1402.6703 .

[119] J. Zornoza, Nucl. Instrum. Methods **725**, 76 (2013), arXiv:1204.5290 .

[120] M. G. Aartsen, *et al.* (IceCube Collaboration), "The IceCube neutrino observatory part IV: Searches for dark matter and exotic particles," (2013), arXiv:1309.7007 .

[121] M. Aartsen, *et al.* (IceCube Collaboration), Phys. Rev. D **88**, 122001 (2013), arXiv:1307.3473 .

[122] M. Doro, *et al.*, J. Astropart. Phys. **43**, 189 (2013).

[123] M. W. Goodman and E. Witten, Phys. Rev. D **31**, 3059 (1985).

[124] A. K. Drukier, K. Freese, and D. N. Spergel, Phys. Rev. D **33**, 3495 (1986).

[125] D. G. Cerdeño and A. M. Green, "Direct detection of WIMPs," in *Particle Dark Matter*, edited by G. Bertone and G. Bertone (Cambridge University Press, Cambridge, 2010) Chap. 17, pp. 347–369, arXiv:1002.1912 .

[126] R. Bernabei, *et al.*, Eur. Phys. J. C **67**, 39 (2010), arXiv:1002.1028 .

[127] C. Aalseth, *et al.* (CoGeNT Collaboration), Phys. Rev. Lett. **106**, 131301+ (2011).

[128] C. E. Aalseth, *et al.*, Phys. Rev. Lett. **107**, 141301+ (2011), arXiv:1106.0650 .

[129] L. Stodolsky, *et al.*, J. Phys.: Conf. Ser. **384**, 012013+ (2012), arXiv:1203.6835 .

[130] J. Engel, S. Pittel, and P. Vogel, Int. J. Mod. Phys. E **01**, 1 (1992).

[131] A. Kurylov and M. Kamionkowski, Phys. Rev. D **69**, 063503 (2003), arXiv:hep-ph/0307185 .

[132] J. Fan, M. Reece, and L.-T. Wang, J. Cosmol. Astropart. Phys. **2010**, 042 (2010), arXiv:1008.1591 .

[133] M. Cirelli, E. D. Nobile, and P. Panci, J. Cosmol. Astropart. Phys. **2013**, 019 (2013), arXiv:1307.5955 .

[134] A. L. Fitzpatrick, W. Haxton, E. Katz, N. Lubbers, and Y. Xu, J. Cosmol. Astropart. Phys. **2013**, 004 (2013), arXiv:1203.3542 .

[135] J. M. Alarcón, J. M. Camalich, and J. A. Oller, Phys. Rev. D **85**, 051503 (2012), arXiv:1110.3797 .

[136] G. S. Bali, *et al.* (QCDSF Collaboration), Phys. Rev. D **85**, 054502 (2012), arXiv:1111.1600 .

[137] M. Shifman, A. Vainshtein, and V. Zakharov, Phys. Lett. B **78**, 443 (1978).

[138] J. Engel, Phys. Lett. B **264**, 114 (1991).

[139] A. Münster, *et al.*, "Radiopurity of CaWO$_4$ crystals for direct dark matter search with CRESST and EURECA," (2014), arXiv:1403.5114 .

[140] R. Bernabei, *et al.*, Nucl. Instrum. Methods A **592**, 297 (2008), arXiv:0804.2738 .

[141] M. Kuźniak, M. Boulay, and T. Pollmann, J. Astropart. Phys. **36**, 77 (2012), arXiv:1203.1576 .

[142] C. Galbiati, *et al.*, J. Phys.: Conf. Ser. **120**, 042015+ (2008), arXiv:0712.0381 .

[143] E. Aprile, T. Yoon, A. Loose, L. W. Goetzke, and T. Zelevinsky, Rev. Sci. Instrum. **84**, 093105+ (2013), arXiv:1305.6510 .

[144] S. Scholl and J. Jochum, J. Phys.: Conf. Ser. **375**, 012020+ (2012).

[145] E. Aprile, *et al.*, J. Phys. G **40**, 115201+ (2013), arXiv:1306.2303 .

[146] Z. Ahmed *et al.* (CDMS Collaboration), (2009), arXiv:0912.3592 .

[147] Z. Ahmed, *et al.* (CDMS Collaboration), Phys. Rev. Lett. **106** (2011), arXiv:1011.2482 .

[148] R. Agnese, *et al.*, Phys. Rev. Lett. **111** (2013), arXiv:1304.4279 .

[149] G. Angloher, *et al.*, Eur. Phys. J. C **72** (2012), arXiv:1109.0702 .

[150] C. E. Aalseth, *et al.*, Phys. Rev. D **88** (2013), arXiv:1208.5737 .

[151] C. E. Aalseth, *et al.*, "Search for an annual modulation in three years of CoGeNT dark matter detector data," (2014), arXiv:1401.3295 .

[152] C. E. Aalseth, *et al.*, "Maximum likelihood signal extraction method applied to 3.4 years of CoGeNT data," (2014), arXiv:1401.6234 .

[153] E. Armengaud, *et al.*, Phys. Lett. B **702**, 329 (2011), arXiv:1103.4070 .

[154] D. Akimov, *et al.*, Phys. Lett. B **709**, 14 (2012), arXiv:1110.4769 .

[155] E. Aprile, *et al.* (XENON Collaboration), Phys. Rev. Lett. **107**, 131302+ (2011), arXiv:1104.2549 .

[156] D. S. Akerib, *et al.* (LUX Collaboration), Phys. Rev. Lett. **112** (2014), arXiv:1310.8214 .

[157] A. Marchionni, *et al.*, J. Phys.: Conf. Ser. **308**, 012006+ (2011), arXiv:1012.5967 .

[158] A. Badertscher, *et al.*, J. Instrum. **8**, C09005+ (2013).

[159] M. Boulay and B. Cai (DEAP/CLEAN Collaboration), Journal of Physics: Conference Series **136**, 042081+ (2008).

[160] E. Behnke, *et al.*, Phys. Rev. Lett. **106**, 021303+ (2011).

[161] M. Felizardo, *et al.* (SIMPLE Collaboration), Phys. Rev. Lett. **108** (2012), arXiv:1106.3014 .

[162] S. Archambault, *et al.* (PICASSO Collaboration), Phys. Lett. B **711**, 153 (2012), arXiv:1202.1240 .

[163] S. K. Kim, H. J. Kim, and Y. D. Kim, New J. Phys. **12**, 075003+ (2010).

[164] R. Bernabei, *et al.*, Eur. Phys. J. C **56**, 333 (2008), arXiv:0804.2741 .

[165] R. Bernabei, *et al.*, Eur. Phys. J. C **73** (2013), arXiv:1308.5109 .

[166] H. S. Lee, *et al.*, Phys. Rev. Lett. **99** (2007), arXiv:0704.0423 .

[167] B. Ahmed, *et al.*, J. Astropart. Phys. **19**, 691 (2003), arXiv:hep-ex/0301039 .

[168] R. Bernabei, *et al.*, Riv. Nuovo Cimento **26**, 1 (2003), arXiv:astro-ph/0307403 .

[169] P. Belli, R. Bernabei, A. Bottino, F. Cappella, R. Cerulli, N. Fornengo, and S. Scopel, Phys. Rev. D **84**, 055014 (2011), arXiv:1106.4667 .

[170] D. Hooper, J. I. Collar, J. Hall, D. McKinsey, and C. Kelso, Phys. Rev. D **82**, 123509+ (2010), arXiv:1007.1005 .

[171] R. Agnese, *et al.*, "Search for Low-Mass WIMPs with SuperCDMS," (2014), arXiv:1402.7137 .

[172] N. Bozorgnia, G. B. Gelmini, and P. Gondolo, J. Cosmol. Astropart. Phys. **2010**, 019 (2010), arXiv:1006.3110 .

[173] K. Blum, "DAMA vs. the annually modulated muon background," (2011), arXiv:1110.0857 .

[174] R. Bernabei, *et al.*, Eur. Phys. J. C **72**, 1 (2012), arXiv:1202.4179 .

[175] M. R. Buckley and W. H. Lippincott, Phys. Rev. D **88**, 056003 (2013), arXiv:1306.2349 .

[176] J. L. Feng, J. Kumar, D. Marfatia, and D. Sanford, Phys. Lett. B **703**, 124 (2011), arXiv:1102.4331 .

[177] D. Smith and N. Weiner, Phys. Rev. D **64**, 043502 (2001), arXiv:hep-ph/0101138 .

[178] R. Foot, Phys. Lett. B **728**, 45 (2014), arXiv:1305.4316 .

[179] T. Schwetz and J. Zupan, J. Cosmol. Astropart. Phys. **2011**, 008 (2011), arXiv:1106.6241 .

[180] E. Aprile, *et al.* (XENON Collaboration), Phys. Rev. Lett. **111** (2013), arXiv:1301.6620 .

[181] E. Aprile, "The Xenon1T dark matter search experiment," in *Sources and Detection of Dark Matter and Dark Energy in the Universe*, Vol. 148, edited by D. Cline (Springer Netherlands, Dordrecht, 2012) Chap. 14, pp. 93–96, arXiv:1206.6288 .

[182] H. Kraus, *et al.*, Nucl. Phys. B: Proc. Suppl. **173**, 168 (2007).

[183] S. Roth, C. Ciemniak, C. Coppi, F. Feilitzsch, A. Gütlein, C. Isaila, J. Lanfranchi, S. Pfister, W. Potzel, and W. Westphal, J. Opt. Mater. **31**, 1415 (2009), arXiv:0810.0423 .

[184] L. Baudis (DARWIN consortium), J. Phys.: Conf. Ser. **375**, 012028+ (2012), arXiv:1201.2402 .

[185] A. Drukier, K. Freese, D. Spergel, C. Cantor, G. Church, and T. Sano, "New dark matter detectors using DNA for nanometer tracking," (2012), arXiv:1206.6809 .

[186] A. Lopez, A. Drukier, K. Freese, C. Kurdak, and G. Tarle, "New dark matter detector using nanoscale explosives," (2014), arXiv:1403.8115 .

[187] A. A. Aguilar-Arevalo, *et al.* (DAMIC Collaboration), "DAMIC: a novel dark matter experiment," (2013), arXiv:1310.6688 .

[188] P. deNiverville, D. McKeen, and A. Ritz, Phys. Rev. D **86**, 035022 (2012), arXiv:1205.3499 .

[189] B. Borasoy and Ulf-G, Phys. Lett. B **365**, 285 (1995), arXiv:hep-ph/9508354 .

[190] M. M. Pavan, I. I. Strakovsky, R. L. Workman, and R. A. Arndt, "The pion-nucleon sigma term is definitely large: results from a G.W.u. analysis of pion nucleon scattering data," (2001), arXiv:hep-ph/0111066 .

[191] L. Alvarez-ruso, T. Ledwig, M. J. Vicente Vacas, and J. Martin-camalich, Int. J. Mod. Phys.: Conf. Ser. **26**, 1460089+ (2014), arXiv:1402.1031 .

[192] J. Ashman, *et al.*, Phys. Lett. B **206**, 364 (1988).

[193] R. L. Jaffe and A. Manohar, Nucl. Phys. B **337**, 509 (1990).

[194] D. Adams, Phys. Rev. D **56**, 5330 (1997), arXiv:hep-ex/9702005 .

[195] D. Qing, X.-S. Chen, and F. Wang, Phys. Rev. C **57**, R31 (1998).

[196] A. Thomas, Phys. Rev. Lett. **101**, 102003+ (2008).

[197] R. Helm, Phys. Rev. **104**, 1466 (1956).

[198] J. D. Lewin and P. F. Smith, Astropart. Phys. **6**, 87 (1996).

[199] G. Fricke, C. Bernhardt, K. Heilig, L. Schaller, L. Schellenberg, E. Shera, and C. Dejager, At. Data. Nucl. Data Tables **60**, 177 (1995).

[200] G. Co', V. De Donno, M. Anguiano, and A. M. Lallena, J. Cosmol. Astropart. Phys. **2012**, 010+ (2012).

[201] C. Ya-Zheng, C. Jun-Mou, L. Yan-An, S. Hong, and L. Xue-Qian, Chin. Phys. C **36**, 505+ (2012).

[202] M. Cannoni, Phys. Rev. D **87**, 075014 (2013), arXiv:1211.6050 .

[203] M. Ressell and D. Dean, Phys. Rev. C **56**, 535 (1997), hep-ph/9702290 .

[204] J. Engel and P. Vogel, Phys. Rev. D **40**, 3132 (1989).

[205] F. Iachello, L. M. Krauss, and G. Maino, Phys. Lett. B **254**, 220 (1991).

[206] J. Ellis and R. A. Flores, Nucl. Phys. B **307**, 883 (1988).

[207] D. G. Cerdeno, M. Fornasa, J.-H. Huh, and M. Peiro, Phys. Rev. D **87**, 023512 (2012), arXiv:1208.6426 .

[208] J. Kumar, Int. J. Mod. Phys.: Conf. Ser. **10**, 115 (2012), arXiv:1201.0217 .

[209] K. Hamaguchi, S. P. Liew, T. Moroi, and Y. Yamamoto, "Isospin-Violating dark matter with colored mediators," (2014), arXiv:1403.0324 .

[210] K. Schmidt-Hoberg, F. Staub, and M. W. Winkler, Phys. Lett. B **727**, 506 (2013), arXiv:1310.6752 .

[211] H. An, L.-T. Wang, and H. Zhang, "Dark matter with t-channel mediator: a simple step beyond contact interaction," (2014), arXiv:1308.0592 .

[212] M. Pospelov and T. T. Veldhuis, Phys. Lett. B **480**, 181 (2000), arXiv:hep-ph/0003010 .

[213] C. M. Ho and R. J. Scherrer, Phys. Lett. B **722**, 341 (2013), arXiv:1211.0503 .

[214] R. Catena and P. Ullio, J. Cosmol. Astropart. Phys. **2010**, 004 (2010), arXiv:0907.0018 .

[215] M. Weber and W. de Boer, Astron. Astrophys. **509**, A25+ (2010), arXiv:0910.4272 .

[216] F. Nesti and P. Salucci, J. Cosmol. Astropart. Phys. **07**, 016 (2013), arXiv:1304.5127 .

[217] S. Garbari, C. Liu, J. I. Read, and G. Lake, Mon. Not. R. Astron. Soc. **425**, 1445 (2012), arXiv:1206.0015 .

[218] F. Iocco, M. Pato, G. Bertone, and P. Jetzer, J. Cosmol. Astropart. Phys. **11**, 029 (2011), arXiv:1107.5810 .

[219] C. Moni Bidin, G. Carraro, R. A. Méndez, and R. Smith, Astrophys. J. **751**, 30+ (2012), arXiv:1204.3924 .

[220] J. Bovy and S. Tremaine, Astrophys. J. **756**, 89 (2012), arXiv:1205.4033 .

[221] A. M. Green, Mod. Phys. Lett. A **27**, 1230004 (2012), arXiv:1112.0524 .

[222] P. Salucci, F. Nesti, G. Gentile, and C. Frigerio Martins, Astron. Astrophys. **523**, A83+ (2010), arXiv:1003.3101 .

[223] F. J. Kerr and D. Lynden-Bell, Mon. Not. R. Astron. Soc. **221**, 1023 (1986).

[224] M. Feast and P. Whitelock, Mon. Not. R. Astron. Soc. **291**, 683 (1997), arXiv:astro-ph/9706293 .

[225] M. C. Smith, *et al.*, Mon. Not. R. Astron. Soc. **379**, 755 (2007), astro-ph/0611671 .

[226] T. Piffl, *et al.*, Astron. Astrophys. **562**, A91+ (2014), arXiv:1309.4293 .

[227] N. W. Evans, C. M. Carollo, and P. T. de Zeeuw, Mon. Not. R. Astron. Soc. **318**, 1131 (2000), arXiv:astro-ph/0008156 .

[228] L. M. Widrow, Astrophys. J. Suppl. Ser. **131**, 39 (2000).

[229] M. Lisanti, L. E. Strigari, J. G. Wacker, and R. H. Wechsler, Phys. Rev. D **83**, 023519 (2011), arXiv:1010.4300 .

[230] P. Bhattacharjee, S. Chaudhury, S. Kundu, and S. Majumdar, Phys. Rev. D **87**, 083525 (2013), arXiv:1210.2328 .

[231] M. Fornasa and A. M. Green, Phys. Rev. D **89** (2013), arXiv:1311.5477 .

[232] M. Vogelsberger, A. Helmi, V. Springel, S. D. M. White, J. Wang, C. S. Frenk, A. Jenkins, A. Ludlow, and J. F. Navarro, Mon. Not. R. Astron. Soc. **395**, 797 (2009), arXiv:0812.0362 .

[233] M. Kuhlen, N. Weiner, J. Diemand, P. Madau, B. Moore, D. Potter, J. Stadel, and M. Zemp, J. Cosmol. Astropart. Phys. **02**, 030 (2010), arXiv:0912.2358 .

[234] Y.-Y. Mao, L. E. Strigari, R. H. Wechsler, H.-Y. Wu, and O. Hahn, Astrophys. J. **764**, 35 (2012), arXiv:1210.2721 .

[235] M. Kuhlen, M. Lisanti, and D. N. Spergel, Phys. Rev. D **86**, 063505 (2012), arXiv:1202.0007 .

[236] J. I. Read, L. Mayer, A. M. Brooks, F. Governato, and G. Lake, Mon. Not. R. Astron. Soc. **397**, 44 (2009), arXiv:0902.0009 .

[237] J. I. Read, *et al.*, AIP Conf. Proc. **1240**, 391 (2010), arXiv:0901.2938 .

[238] A. M. Green, J. Cosmol. Astropart. Phys. **10**, 034 (2010), arXiv:1009.0916 .

[239] A. H. G. Peter, Phys. Rev. D **83**, 125029 (2011), arXiv:1103.5145 .

[240] M. Fairbairn, T. Douce, and J. Swift, J. Astropart. Phys. **47**, 45 (2013), arXiv:1206.2693 .

[241] L. E. Strigari and R. Trotta, J. Cosmol. Astropart. Phys. **2009**, 019 (2009), arXiv:0906.5361 .

[242] A. H. G. Peter, Phys. Rev. D **81**, 087301+ (2010), arXiv:0910.4765 .

[243] C. Arina, G. Bertone, and H. Silverwood, Phys. Rev. D **88** (2013), arXiv:1304.5119 .

[244] M. Pato, L. Baudis, G. Bertone, R. R. de Austri, L. E. Strigari, and R. Trotta, Phys. Rev. D **83** (2011), arXiv:1012.3458 .

[245] M. Pato, L. E. Strigari, R. Trotta, and G. Bertone, J. Cosmol. Astropart. Phys. **2013**, 041 (2013), arXiv:1211.7063 .

[246] M. Drees and C.-L. Shan, J. Cosmol. Astropart. Phys. **2007**, 011 (2007), arXiv:astro-ph/0703651 .

[247] M. Drees and C.-L. Shan, J. Cosmol. Astropart. Phys. **2008**, 012+ (2008), arXiv:0803.4477 .

[248] B. Feldstein and F. Kahlhoefer, "A new halo-independent approach to dark matter direct detection analysis," (2014), arXiv:1403.4606 .

[249] P. J. Fox, J. Liu, and N. Weiner, Phys. Rev. D **83** (2011), arXiv:1011.1915 .

[250] M. T. Frandsen, F. Kahlhoefer, C. McCabe, S. Sarkar, and K. Schmidt-Hoberg, J. Cosmol. Astropart. Phys. **2012**, 024 (2012), arXiv:1111.0292 .

[251] P. Gondolo and G. B. Gelmini, J. Cosmol. Astropart. Phys. **2012**, 015 (2012), arXiv:1202.6359 .

[252] E. D. Nobile, G. Gelmini, P. Gondolo, and J.-H. Huh, J. Cosmol. Astropart. Phys. **2013**, 048 (2013), arXiv:1306.5273 .

[253] P. Gondolo, Phys. Rev. D **66** (2002), arXiv:hep-ph/0209110 .

[254] C. J. Copi, J. Heo, and L. M. Krauss, Phys. Lett. B **461**, 43 (1999), arXiv:hep-ph/9904499 .

[255] C. J. Copi and L. M. Krauss, Phys. Rev. D **67** (2002), arXiv:astro-ph/0208010 .

[256] B. Morgan, A. Green, and N. Spooner, Phys. Rev. D **71**, 103507 (2005), arXiv:astro-ph/0408047 .

[257] E. Daw, *et al.*, Astropart. Phys. **35**, 397 (2012), arXiv:1010.3027 .

[258] E. Daw, *et al.*, EAS Publ. Ser. **53**, 11 (2012), arXiv:1110.0222 .

[259] K. Miuchi, *et al.*, Phys. Lett. B **686**, 11 (2010), arXiv:1002.1794 .

[260] K. Miuchi, *et al.*, EAS Publ. Ser. **53**, 33 (2012), arXiv:1109.3099 .

[261] Q. Riffard, *et al.*, "Dark matter directional detection with MIMAC," (2013), arXiv:1306.4173 .

[262] D. Santos, *et al.*, J. Phys.: Conf. Ser. **469**, 012002+ (2013), arXiv:1311.0616 .

[263] J. Monroe (DMTPC Collaboration), EAS Publ. Ser. **53**, 19 (2012).

[264] J. B. R. Battat (DMTPC Collaboration), J. Phys.: Conf. Ser. **469**, 012001+ (2013).

[265] S. Vahsen, H. Feng, M. Garcia-Sciveres, I. Jaegle, J. Kadyk, Y. Nguyen, M. Rosen, S. Ross, T. Thorpe, and J. Yamaoka, EAS Publ. Ser. **53**, 43 (2012).

[266] J. Billard, F. Mayet, and D. Santos, J. Cosmol. Astropart. Phys. **2012**, 006 (2012), arXiv:1202.3372 .

[267] S. Burgos, *et al.*, Astropart. Phys. **31**, 261 (2008), arXiv:0809.1831 .

[268] A. Green and B. Morgan, Phys. Rev. D **77**, 027303 (2008).

[269] T. Naka, M. Kimura, M. Nakamura, O. Sato, T. Nakano, T. Asada, Y. Tawara, and Y. Suzuki, EAS Publ. Ser. **53**, 51 (2012), arXiv:1109.4485 .

[270] S. Ahlen, *et al.*, Int. J. Mod. Phys. A **25**, 1 (2009), arXiv:0911.0323 .

[271] D. S. M. Alves, S. E. Hedri, and J. G. Wacker, "Dark matter in 3D," (2012), arXiv:1204.5487 .

[272] M. Kuhlen, J. Diemand, P. Madau, and M. Zemp, J. Phys.: Conf. Ser. **125**, 012008+ (2008), arXiv:0810.3614 .

[273] S. K. Lee, "Harmonics in the Dark-Matter sky: Directional detection in the Fourier-Bessel basis," (2014), arXiv:1401.6179 .

[274] S. Helgason, *The Radon Transform*, 2nd ed. (Birkhauser, Boston, 1999).

[275] E. T. Quinto, J. Math. Anal. Appl. **91**, 510 (1983).

[276] L. A. Shepp and J. B. Kruskal, Amer. Math. Soc. **85**, 420 (1978).

[277] E. T. Quinto, J. Math. Anal. Appl. **90**, 408 (1982).